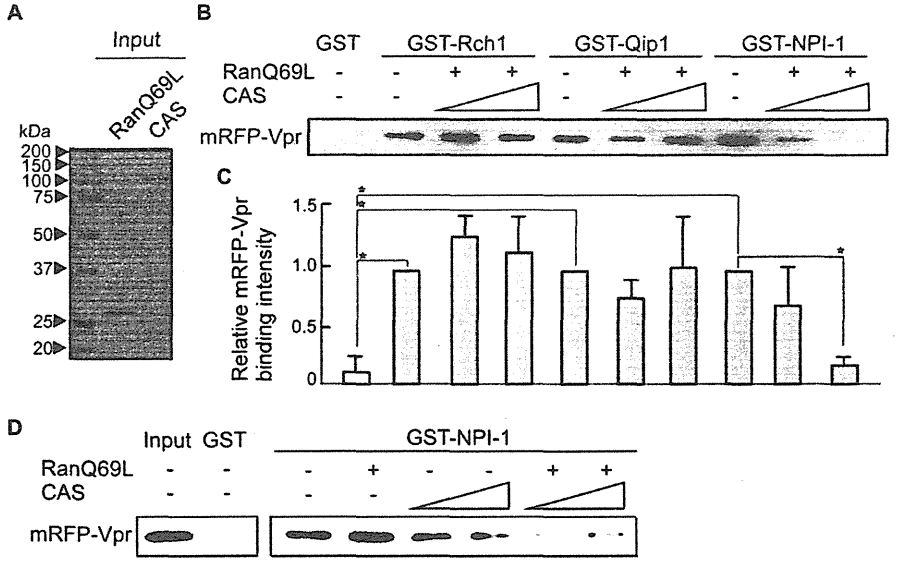

Figure 4. CAS disrupts the interaction between Vpr and NPI-1. (A) *Twenty-five pmol of purified recombinant* RanQ69L and CAS were resolved by 10% SDS-PAGE and stained with CBB. (B) Glutathione-Sepharose beads coupled with the GST-Impα isoforms, Rch1, Qip1 and NPI-1 (each 25 pmol) or GST (25 pmol), were incubated with mRFP-Vpr, Q69LRanGTP (25 pmol) and/or CAS protein (5 and 50 pmol, respectively). The bound fractions of mRFP-Vpr and mRFP were analyzed by immunoblotting with anti-Flag M2 MAb. (C) The immunoblots of mRFP-Vpr binding were analyzed by densitometry and each sample was normalized to the Impα isoforms without CAS protein. Each column and error bar represents the means ± SD of results from three experiments. The asterisk* represents a *p*-value of <0.0005. (D) Glutathione-Sepharose beads coupled with the NPI-1 (each 25 pmol) or GST (25 pmol), were incubated with mRFP-Vpr, Q69LRanGTP (25 pmol) and/or CAS protein (10 and 50 pmol, respectively). The bound fractions of mRFP-Vpr were analyzed by immunoblotting with anti-Flag M2 MAb. The bound fractions and 1/20 of the input of mRFP-Vpr were analyzed by immunoblotting with anti-Flag M2 MAb. The positions of mRFP-Vpr are indicated.
doi:10.1371/journal.pone.0027815.g004

by Rch1 or Qip1, in contrast to the import of Vpr_{N17C74} by all three isoforms of Impα (**Fig. 1B**) [6]. In addition, the NPI-1–driven nuclear import of Vpr appeared to be completely inhibited when Impβ was added to the *in vitro* import assay as shown in **Fig. 1E**. Thus, it seems that the transport of full-length Vpr is mediated in an Impα-dependent/Impβ-independent manner, as was found previously for Vpr_{N17C74} [5,6]. vii) In an *in vitro* nuclear import assay using HeLa cells with knocked-down CAS, we showed that CAS promotes the NPI-1–mediated nuclear import of Vpr. Taken together, the results suggested that the differences in the dissociation rates for the interactions between Vpr and the three Impα isoforms might permit the novel nuclear import of full-length Vpr specifically mediated by NPI-1. Data from the present study leads us to speculate that the Vpr N- or C-terminal region will bind to the ninth ARM region of Impα with the potential regulation of the nuclear import process through the dissociation of Vpr from NPI-1 via an interaction with CAS. Indeed, it has been reported that the C-terminal region of Vpr, which most closely resembles a classical NLS, is highly involved in its nuclear localization [**39,40**].

It is unclear how the selective release of full-length Vpr from NPI-1 depends on CAS; however, there two possible hypotheses with regards to its mechanism: first, it is predicted that since the binding affinities of Vpr for the C-terminal domain were almost the same for all three Impα isoforms, CAS must be attracted to specific amino acids in NPI-1. Interestingly, the alignment of the sequences of the ninth ARM motif, which are involved in the binding of Vpr, showed that the three Impα isoforms share only 50% overall amino acid sequence similarity [2,11,12], suggesting that the ARM motif of NPI-1 may be more effective at binding CAS than that of Rch1 or Qip1. The second possibility relates to the targeting of Vpr to the perinuclear region. Sun *et al.* [38] showed that Impα/NLS cargo complexes, without Impβ, dissociated in the presence of CAS and RanGTP at the nuclear pore complexes. They also speculated that Nup50 facilitates the dissociation of Impα/NLS cargo complexes in the presence of CAS and RanGTP when it reaches the nuclear basket region of the NPC [38]. In a recent report, Ogawa *et al.* [9] speculated that the dissociation of Impα from the NLS-substrate was promoted by Npap60 (Nup50). In addition, interactions between transport factors and key nucleoporins, such as Nup1p, Nup2p and Nup50, appeared to accelerate the formation and dissociation of the NLS cargo/Impα/Impβ complexes [38]. Likewise, in this study, we have also shown that the dissociation of the Vpr/NPI-1complexes may occur at the perinuclear region using an *in vitro* nuclear import assay with digitonin-permeabilized HeLa cells. In this assay, full-length Vpr was targeted directly to the perinuclear region in the absence of soluble factors, and, in addition, this perinuclear localization increased in a dose-dependent manner upon the addition of NPI-1. Earlier studies confirmed that Vpr can interact with nuclear pore complex components [15,16,27,41] and we have previously demonstrated that the interaction between Vpr and the NPC is crucial for Vpr nuclear import, since Vpr mutants, with barely detectable perinuclear localization, could not be imported into the nucleus [5]. Further studies on the role of Vpr at the NPC are now essential for a full understanding of the mechanism of CAS-regulated, NPI-1–mediated nuclear import of full-length Vpr.

Our results clearly indicate that the ninth ARM repeat region of all of three Impα isoforms is the major binding site for full-length Vpr. In contrast, we here demonstrate that the IBB domain of Impα interacts with full-length Vpr, albeit with lower affinity than

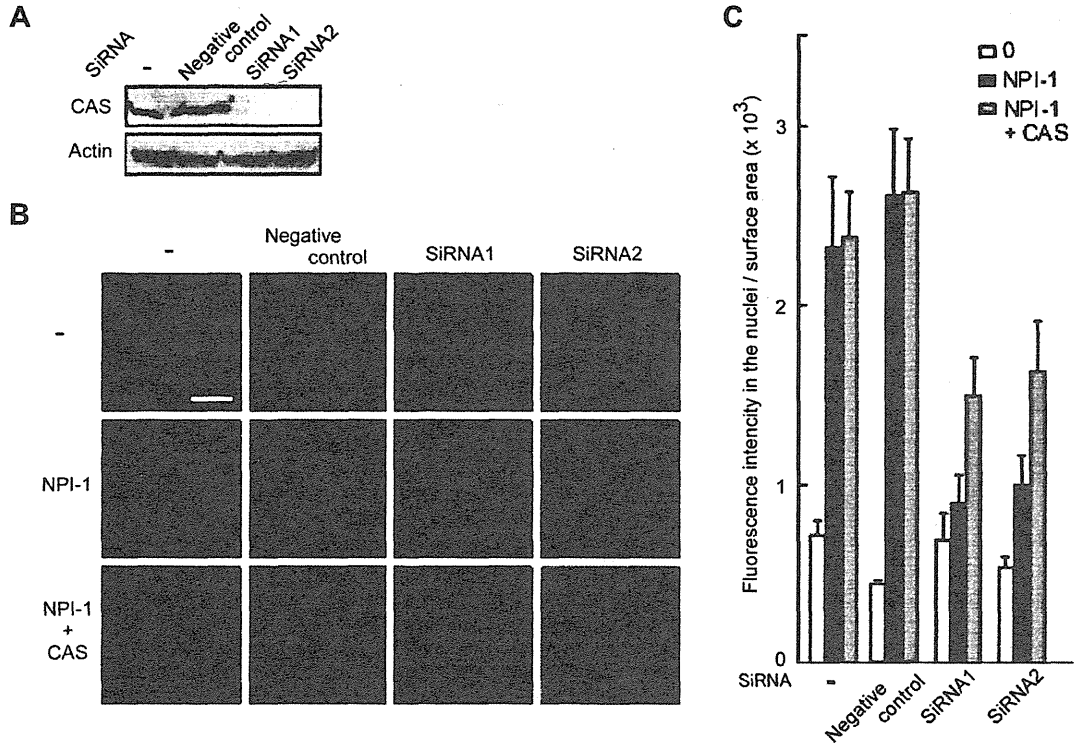

Figure 5. The siRNA-induced knock down of CAS prevents the nuclear import of Vpr. (A) CAS-specific siRNA and nonspecific siRNA (negative control) transfections were performed in HeLa cells. After 36 h of treatment with CAS-specific siRNA1 and siRNA2 and the negative control siRNA, cell extracts were prepared and immunoblotting with an anti-CAS antibody was used to determine the transfection efficiencies of the siRNAs. Untreated HeLa cells (-). Actin was included as an internal control. The positions of CAS and actin are indicated. (B) Digitonin-permeabilized HeLa cells, transfected with siRNAs, were incubated with 1 μM GST-GFP-Vpr, 1 μM NPI-1 and 1 μM CAS. After fixation, cells were analyzed by confocal laser scanning microscopy. Bar = 10 μm. (C) Fluorescence intensity per nuclear surface area was quantified in over 80 nuclei from three independent experiments. The bar shows the standard errors of measurements.
doi:10.1371/journal.pone.0027815.g005

those shown by the full-length Impα isoforms to their C-terminal domains. This result partially corresponds to our previous finding that Impα binds strongly to Vpr_{N17C74} via the IBB domain, but this binding is not essential for the nuclear entry of Vpr [5]. The IBB domain contains an NLS-like sequence (49-KRRNV-53) that binds to autologous NLS-binding sites in a similar way to the NLS of SV40. Thus, Impα appears to be prevented from binding to a classical-type NLS by an internal NLS until Impβ binds to the IBB domain [42]. These facts suggest that Vpr might modulate the interaction between a classical NLS-bearing protein and Impα, as does Impβ. Interestingly, Bukrinsky and colleagues [16,43] reported that Vpr associates with the N-terminal region of Impα, which overlaps with the IBB domain of Impα and differs from the classical NLS cargo binding site. This interaction may stimulate nuclear import of the cargo by increasing the affinity of Impα for NLS-containing proteins, including that of HIV-1 matrix (MA) protein, which is one of the components of the PIC and has a basic type of NLS. Thus, Vpr might accelerate nuclear import of the PIC through interaction with the IBB domain, in addition to the NPI-1-driven nuclear import of Vpr, that requires the C-terminal domain of Impα.

Various factors are reported to adapt Impα isoforms for nuclear import. Viral proteins, such as the herpes virus open reading frame (ORF) 57 protein [44], the Influenza virus nucleoprotein [45,46], and polymerase PB2 [47], appear to be transported by NPI-1. Likewise, it was recently shown that HIV-1 IN appears to interact with Qip1 and contributes to the nuclear import of PIC and viral replication [35]. The results of the present study show that Vpr is selectively imported into the nucleus by NPI-1, and previous work shows that the interaction between Impα and Vpr is necessary not only for the nuclear import of Vpr but also for HIV-1 replication in macrophages [48]. Macrophages are a major target for HIV-1 and serve as a viral reservoir that releases small amounts of viral particles in symptomatic carriers [49]. A striking feature of HIV-1 is its ability to replicate in non-dividing cells, particularly in macrophages. Replication in non-dividing cells depends on the active nuclear import of the viral PIC, which includes the viral proteins, IN, Vpr, and small amounts of MA, in addition to viral nucleic acids [48]. Vpr is particularly important for the nuclear import of the PIC in non-dividing cells [6,14,15,24], although its exact role in the PIC entry mechanism remains to be clarified. Work is currently ongoing to study the expression of Impβ in human differentiated macrophages, and preliminary data suggest that it is expressed at very low levels in primary differentiated macrophages. The low level of Impβ expression in macrophages may result in the inefficient nuclear import of MA and IN, which utilize the classical Impα/Impβ-dependent nuclear import pathway. By contrast, previous studies show that all three Impα isoforms are strongly expressed at both the mRNA and protein levels [6]. This suggests that, although Vpr utilizes many nuclear import pathways [6,16,26,27,28], the Impα-mediated nuclear import pathway is the most efficient in macrophages. In summary,

the results of the present study show for the first time that CAS mediates the release of Vpr from the Vpr-NPI-1 complex, thereby allowing its transport into the nucleus. Further investigation of the molecular mechanisms underlying the Vpr/NPI-1 interaction and the selective release of full-length Vpr from NPI-1 and its contribution to HIV-1 replication is required to facilitate a better understanding of the HIV-1 nuclear import process.

Materials and Methods

Cell culture

Human cervical HeLa and 293T cells were grown in Dulbecco's modified Eagle's medium (DMEM; Invitrogen, Carlsbad, CA) supplemented with 10% heat-inactivated fetal bovine serum (FBS; Sigma-Aldrich, St. Louis, MO) and GlutaMax (GIBCO Industries Inc., Los Angeles, CA).

Plasmids

The following plasmids have been described previously: the expression vector, pME18Neo, encoding Flag-tagged wild-type Vpr and its control vector, pME18Neo; the expression vector, pCAGGS, encoding Flag-mRFP-Flag-Vpr (mRFP-Vpr) and its control vector, pCAGGS-Flag-mRFP (mRFP); and the GST expression vector, pGEX-6P-3, encoding GST-tagged-Rch1, -Qip1, -NPI-1 and -Impß [6,33,50,51]. The pCAGGS encoding Flag-mRFP-Vpr$_{N17C74}$ (mRFP-N17C74) was constructed as described previously [50]. For the construction of the expression vector pGEX-6P-3, encoding GST-tagged-Vpr (GST-Vpr), a fragment encoding Vpr was amplified by PCR with the following primers: 5′-GGGGATCCGAACAAGCCCCAGAAGACC-3′ and 5′-CCCTCGAGCTAGGATCTACTGGCTCC-3′ from pME18Neo-Flag tagged Vpr [33,51] and was subcloned into pGEX-6P-3 (GE Health, Buckinghamshire, UK) at the *Bam*HI/*Xho*I sites. For construction of the expression vector, GST-green fluorescent protein (GFP)-tagged Vpr (GST-GFP-Vpr), a cDNA encoding histidine tag$_6$ (His$_6$)-tagged-Vpr (Vpr-His), was amplified from pME18Neo-Flag tagged Vpr by PCR with the primers 5′-GGGATCCATGGAACAAGCCCCAGAAGA-3′ and 5′-GCG-GCCGCTCAATGATGATGATGATGATGACCGGTCCCG-GGGGATCTACT-3′ and subcloned into the pGEX-6P-1-GFP vector at the *Bam*HI/*Not*I sites. The plasmid GST-Vpr$_{N17C74}$-GFP (GST-N17C74-GFP) has been described previously [5]. To construct the expression vector, pGEX-6P-3-CAS, a cDNA encoding CAS was prepared from pGEX-6P-2-GFP-CAS [9] and ligated into pGEX-6P-3 at the *Bam*HI/*Xho*I sites. To construct the expression vector, pGEX-6P-3- Q69LRan, a cDNA encoding wild-type Ran was cloned by PCR from a HeLa cDNA library generated using SuperScript II (Invitrogen) according to the manufacturer's instructions. The N-terminal His-tag fused Ran was then amplified by PCR and subcloned into pGEX-6P-3 (GE Healthcare Life Science). Q69LRan was generated using a QuickChange II Site-Directed Mutagenesis kit (Stratagene) according to the manufacturer's instructions. For construction of the truncated Impα isoform expression vectors, the fragments were amplified by PCR and were subcloned into pGEX-6P-3 at the *Bam*HI/*Eco*RI sites for Rch1 and NPI-1 and the *Bam*HI/*Xho*I sites for Qip1. The following PCR primers were used: Rch1 1-69, 5′-CCCGGATCCTCCACCAACGAGAATGCTAATACACC-3′ and 5′-CCCGAATTCCTAGTTGCGGTTTTCCTGCAGC-GG-3′; 70-475, 5′-CCCGGATCCAACCAGGGCACTGTAA-ATTGG-3′ and 5′-GGGGAATTCCTAAGCTTCAATTT-TGTCTAA -3′; 70–402, 5′-CCCGGATCCAACCAGGGCAC-TGTAAATTGG-3′ and 5′-CCCGAATTCCTAGTTGGT-CACGGCCCACACAGCTTCC-3′; 403–529, 5′-GGGGGATC-CTATACCAGTGGTGGAACAG-3′ and 5′-GGGGAATTCC-TAAAAGTTAAAGGTCCC-3′; NPI-1 1–75, 5′-CCCGGATC-CACCACCCCAGGAAAAGAGAAC-3′ and 5′-GGGGAATT-CCTACATGTTATTAATCTGAGCCTCATG-3′; 76–405, 5′-CCCGGATCCGAGATGGCACCAGGTGGTGTC-3′ and 5′-CCCGAATTCTCAGGCCCAAGCTGCTTCTTTTCTTG-3′; 76–451, 5′-CCCGGATCCGAGATGGCACCAGGTGGTGT-C-3′ and 5′-GGGGAATTCTCACAGGATATTTTCCAAG-CC-3′; 406–538, 5′-CCCGGATCCATCACAAATGCAACT-TCTGG-3′ and 5′-GGGGAATTCTCAAAGCTGGAAACC-TTCCATAG-3′; Qip1 1–67, 5′-CCCGGATCCGCGGACAAC-GAGAAACT-3′ and 5′-GGGCTCGAGCTATCTATAAT-CACCATCTATATCAGAG-3′; 68–393, 5′-CCCGGATCCGT-GCAAAATACCTCTCTAGAA-3′ and 5′-GGGGCTCGAGC-TAGGCCCAAGCAGCTTCTTTTTGAGTGC-3′, 68–439, 5′-CCCGGATCCGTGCAAAATACCTCTCTAGAA-3′ and 5′-GGGGCTCGAGCTACTAATATATTACTTAG-3′; and 394–521, 5′-CCCGGATCCATAAGTAACTTAACAATTAGT-3′ and 5′-GGGCTCGAGCTAAAACTGGAACCCTTCTGTT-GGTAC-3′.

Protein expression and purification

The recombinant GST-tagged Rch1, Qip1, NPI-1, the deletion mutants, GST-GFP, Impß and CAS were expressed in the *Escherichia coli* strain BL21 CodonPlus (DE3)-RIL (Stratagene, La Jolla, CA) and purified using the Glutathione Sepharose 4FF bead system (GSH System, Amersham Biosciences, Piscataway, NJ) as described elsewhere [6,50]. GST-Vpr and GST-GFP-Vpr were purified as described elsewhere [52]. After expressing these proteins in *E. coli*, cells were lyzed with Lysis Buffer [10 mM Tris-HCl (pH 8.0), 500 mM NaCl, 1% Triton X-100, 5 mM 2-Mercaptoethanol, 10% (w/v) glycerol and protein inhibitor]. GST-Vpr and GST-GFP-Vpr were purified using the GSH system (Amersham Biosciences) and separated on a His-Trap column (GE Health) [5,52]. GST-N17C74-GFP protein was purified as described previously [5]. Purified GST-Vpr, GST-GFP-Vpr and GST-N17C74-GFP proteins were dialyzed against transport buffer [TB: 20 mM HEPES-KOH [pH 7.3], 110 mM potassium acetate, 2 mM magnesium acetate, 5 mM sodium acetate and 1 mM dithiothreitol (DTT)]. RanQ69L was expressed from pGEX-6P-3 and purified on GSTrap and HisTrap column (GE Healthcare), and after nucleotide exchange for GTP, GST was digested by PreScission Protease and separated on Hi-Trap SP column (GE Healthcare). Activity was confirmed by binding with GST-Importin β.

To express and purify the Flag fusion proteins, 293T cells (5×10^5 cells) were transfected with 5 mg of the pCAGGS mammlaian expression vector encoding mRFP-Vpr, mRFP-N17C74 or mRFP using FuGene HD Transfection Reagent (Roche Diagnostics, Basel, Switzerland). Two days after transfection, expressed proteins were purified using ANTI-FLAG M2 agarose (Sigma-Aldrich) as described previously [50].

In vitro nuclear import assay

HeLa cells (2×10^6) were seeded on an eight-well coverslip in a 10-cm dish. After 16 to 24 h of culture, HeLa cells were permeabilized by digitonin in TB on ice for 5 min and washed twice with TB as described previously [25]. The permeabilized cells were incubated at room temperature for 1 h or 30 min with 1% bovine serum albumin, GST-GFP-Vpr (for 1 h), GFP-GST (for 1 h) or GST-N17C74-GFP (for 30 min), and transport substrates in a total volume of 10 µl per sample. After incubation, the cells were washed twice with TB and fixed in 3.7% formaldehyde in TB. Samples were examined using confocal laser

scanning microscopy (FV 1000; Olympus, Tokyo, Japan) and the nuclear fluorescence intensity was analyzed with MetaMorph software (Molecular Devices Inc., Downingtown, PA). For each condition, the fluorescence intensity per nuclear surface area was quantified for at least 70 nuclei stained with Hoechst 33342 (ImmunoChemistry Technologies LLC., Bloomington, MN).

Pull-down assay

Glutathione-Sepharose 4FF beads were coupled with GST-Impα isoforms and their mutants in TB for 1 h at 4°C and then in 10 mM Tris-HCl (pH 8.0), 50 mM NaCl, 0.05% NP-40 and 1 mM DTT. Vpr proteins purified from 293T cells transfected with pCAGGS encoding mRFP or mRFP-Vpr were incubated with GST-protein conjugated beads for 2 h at 4°C. The beads were washed four times with 500 µl washing buffer [10 mM Tris-HCl (pH 8.0), 150 mM NaCl, 0.2% NP-40 and 1 mM DTT] and bound proteins were eluted by incubation with sodium lauryl sulfate (SDS) sample buffer [100 mM sodium phosphate (pH 7.2), 1% SDS, 10% glycerol, 100 mM DTT and 0.001% bromophenol blue] at 98°C for 5 min. Eluted proteins were fractionated by 10% SDS-polyacrylamide gel electrophoresis (PAGE) and detected by Western blotting with anti-Flag M2 monoclonal antibody (MAb) (Sigma-Aldrich).

Immunoblotting

Cells or proteins were dissolved in SDS sample buffer, heat-denatured and loaded onto 10% SDS polyacrylamide gels. Separated proteins were transferred to a polyvinylidene difluoride membrane (Immobilon; Millipore, Bedford, MA). After treatment with PBST [20 mM Dulbecco's phosphate-buffered saline (PBS) and 0.05% (v/v) Tween 20] containing 5% skim milk at room temperature for 1 h, the blotted membrane was incubated with anti-Flag MAb (M2) (Sigma-Aldrich), anti-CAS polyclonal antibody (CSE1L, Medical & Biological Laboratories Co. Ltd., Nagoya, Japan), or anti-actin polyclonal antibody (Santa Cruz Biotechnology Inc., Santa Cruz, CA) diluted with PBST containing 3% skim milk at room temperature for 2 h or at 4°C for 16 to 18 h. The membrane was rinsed with PBST and incubated with horseradish-peroxidase (HRP)-conjugated goat anti-mouse IgG (Zymed Laboratories, San Francisco, CA) for anti-Flag, HRP-goat anti-rabbit IgGs (Zymed Laboratories) for anti-CAS, or HRP-rabbit anti-goat IgG (Zymed Laboratories) for anti-actin. Each antibody was diluted with PBST containing 3% skim milk. After washing with PBST, the bound antibodies were visualized with ECL™ Blotting Detection Reagents (Amersham Biosciences) followed by exposure to X-ray film (Kodak BioMax™ XAR film, Sigma-Aldrich).

Surface plasmon resonance (SPR) analysis

SPR experiments were performed using the BIAcore 2000 system (GE Health) at room temperature. Impα isoforms and their mutants were coupled directly to the sensor chip (CM5 research grade, GE Health) via standard N-hydroxysuccinimide and N-ethyl-N-(dimethylaminopropyl) carbodiimide activation. To immobilize the proteins, full-length Rch1 [dissolved in 10 mM sodium acetate buffer (pH 5.0)] full-length Qjp1 and full-length NPI-1 [dissolved in 10 mM sodium acetate buffer (pH 4.5)], and their mutants [dissolved in 10 mM sodium acetate buffer (pH 4.0)] were injected onto the sensor surface with HBS EP buffer [10 mM Hepes (pH 7.4), 150 mM NaCl, 3 mM ethylenediaminetetraacetic acid, and 0.05% surfactant P20; GE Healthcare] employed as the mobile phase buffer during the immobilization process. Following immobilization, 50 mM Tris-HCl buffer (pH 7.5) was injected to quench the unreacted N-hydroxysuccinimide groups, and then PBS was used as the mobile phase buffer. GST and GST-Vpr samples at various concentrations were injected as analytes, and bound analytes were subsequently removed by washing with the mobile phase buffer at 300 s after the injection. Vpr sensorgrams were obtained by subtracting GST curves from GST-Vpr curves. Kinetic constants were calculated from the Vpr sensorgrams using the BIA evaluation software, version 3.0 Biacore AB (GE Healthcare). Dissociation constants (K_D) were calculated from the resonance unit at equilibrium using the following equation:

$$R_{eq} = \frac{R_{eq} \cdot C}{C + K_D}$$

where R_{eq} is the steady state binding level, K_D is the dissociation constant and C is the analyte concentration. R_{eq} is related to concentration according to this equation.

Small interfering RNAs (siRNA)

The siRNAs against CAS were designed with the BLOCK-iT RNAi Designer (Invitrogen). The siRNA forward sequences targeting CAS were 5′-AGCAACAGUGGAUAAUUCU-GAUUUC-3′ for siRNA1 and 5′-UUAACUGCUUCUGAAU-UUGCUCUGG-3′ for siRNA2. HeLa cells (1×10^6) were seeded on a 6-cm dish. After cells had adhered to the dish, the cells were transfected with the siRNAs using Lipofectamine RNAiMAX (Invitrogen) according to the manufacturer's protocols. After 16 h, cells (2×10^6) were seeded onto an eight-well coverslip within a 10-cm dish and were used in an *in vitro* import assay following 36 h incubation with an siRNA.

Statistical methodology

Statistical analyses were conducted using R version 2.8 (1).

Supporting Information

Figure S1 Immunofluorescent staining of endogenous CAS in semi-intact cells. The two panels show the steps involved in cell preparation for the *in vitro* import assay: intact cells (left panel), digitonin-treated cells and the cells incubated on ice for 5 min following digitonin treatment (right panel). Cells on cover slips were fixed with 3.7% formaldehyde in PBS for 15 min at room temperature and permeabilized with PBS containing 0.5% Triton X-100 for 7 min on ice. The cells on the coverslips were incubated with either anti-CAS polyclonal antibody (Green) or anti-Rch1 MAb (Red) in PBS containing 5% skim milk for 1 h at RT. After rinsing with PBS, the cells were incubated with either Alexa-488–conjugated anti-rabbit IgG (for CAS) or Alexa-546–conjugated anti-mouse IgG (for Rch1) antibodies (Invitrogen), or Hoechst 33342 (ImmunoChemistry Technologies LLC.) in PBS containing 5% skim milk for 30 min. After rinsing with PBS, the cover slips were mounted on glass slides in PBS containing 90% glycerol before analysis by confocal laser scanning microscopy. Bar = 10 µm.
(TIF)

Acknowledgments

We thank Dr Kazuo Kurokawa and Mr Genta Kitahara for kind help and suggestions concerning the immunofluorescent staining and Drs Yoshihiro Yoneda, Yoshinari Yasuda and Tomohiro Sekimoto for kindly providing the CAS and Impα isoform expression vectors. We are grateful to the Support Unit for Bio-material Analysis, RIKEN BSI Research Resources Center, for help with the BIAcore 2000 analysis and sequence analysis. This work was supported in part by a Health Sciences Research Grant from the Ministry of Health, Labor and Welfare of Japan (Research on HIV/AIDS) and by the program for Promotion of Fundamental Studies in Health Sciences of the National Institute of Biomedical Innovation (NIBIO) of Japan.

Author Contributions

Conceived and designed the experiments: YA ET. Performed the experiments: ET TM GA HM YA. Analyzed the data: ET TM ZM TZ MM YA. Contributed reagents/materials/analysis tools: YA ET TM GM. Wrote the paper: YA ET.

References

1. Gorlich D, Mattaj IW (1996) Nucleocytoplasmic transport. Science 271: 1513–1518.
2. Goldfarb DS, Corbett AH, Mason DA, Harreman MT, Adam SA (2004) Importin alpha: a multipurpose nuclear-transport receptor. Trends Cell Biol 14: 505–514.
3. Fried H, Kutay U (2003) Nucleocytoplasmic transport: taking an inventory. Cell Mol Life Sci 60: 1659–1688.
4. Miyamoto Y, Hieda M, Harreman MT, Fukumoto M, Saiwaki T, et al. (2002) Importin alpha can migrate into the nucleus in an importin beta- and Ran-independent manner. EMBO J 21: 5833–5842.
5. Kamata M, Nitahara-Kasahara Y, Miyamoto Y, Yoneda Y, Aida Y (2005) Importin-alpha promotes passage through the nuclear pore complex of human immunodeficiency virus type 1 Vpr. J Virol 79: 3557–3564.
6. Nitahara-Kasahara Y, Kamata M, Yamamoto T, Zhang X, Miyamoto Y, et al. (2007) Novel nuclear import of Vpr promoted by importin alpha is crucial for human immunodeficiency virus type 1 replication in macrophages. J Virol 81: 5284–5293.
7. Kotera I, Sekimoto T, Miyamoto Y, Saiwaki T, Nagoshi E, et al. (2005) Importin alpha transports CaMKIV to the nucleus without utilizing importin beta. EMBO J 24: 942–951.
8. Herold A, Truant R, Wiegand H, Cullen BR (1998) Determination of the functional domain organization of the importin alpha nuclear import factor. J Cell Biol 143: 309–318.
9. Ogawa Y, Miyamoto Y, Asally M, Oka M, Yasuda Y, et al. (2010) Two isoforms of Npap60 (Nup50) differentially regulate nuclear protein import. Mol Biol Cell 21: 630–638.
10. Hu J, Wang F, Yuan Y, Zhu X, Wang Y, et al. (2010) Novel importin-alpha family member Kpna7 is required for normal fertility and fecundity in the mouse. J Biol Chem 285: 33113–33122.
11. Kelley JB, Talley AM, Spencer A, Gioeli D, Paschal BM (2010) Karyopherin alpha7 (KPNA7), a divergent member of the importin alpha family of nuclear import receptors. BMC Cell Biol 11: 63.
12. Yasuhara N, Oka M, Yoneda Y (2009) The role of the nuclear transport system in cell differentiation. Semin Cell Dev Biol 20: 590–599.
13. Yasuhara N, Shibazaki N, Tanaka S, Nagai M, Kamikawa Y, et al. (2007) Triggering neural differentiation of ES cells by subtype switching of importin-alpha. Nat Cell Biol 9: 72–79.
14. Bukrinsky M, Adzhubei A (1999) Viral protein R of HIV-1. Rev Med Virol 9: 39–49.
15. Vodicka MA, Koepp DM, Silver PA, Emerman M (1998) HIV-1 Vpr interacts with the nuclear transport pathway to promote macrophage infection. Genes Dev 12: 175–185.
16. Popov S, Rexach M, Zybarth G, Reiling N, Lee MA, et al. (1998) Viral protein R regulates nuclear import of the HIV-1 pre-integration complex. EMBO J 17: 909–917.
17. Emerman M (1996) HIV-1, Vpr and the cell cycle. Curr Biol 6: 1096–1103.
18. Goh WC, Rogel ME, Kinsey CM, Michael SF, Fultz PN, et al. (1998) HIV-1 Vpr increases viral expression by manipulation of the cell cycle: a mechanism for selection of Vpr in vivo. Nat Med 4: 65–71.
19. Poon B, Grovit-Ferbas K, Stewart SA, Chen IS (1998) Cell cycle arrest by Vpr in HIV-1 virions and insensitivity to antiretroviral agents. Science 281: 266–269.
20. Kino T, Gragerov A, Slobodskaya O, Tsopanomichalou M, Chrousos GP, et al. (2002) Human immunodeficiency virus type 1 (HIV-1) accessory protein Vpr induces transcription of the HIV-1 and glucocorticoid-responsive promoters by binding directly to p300/CBP coactivators. J Virol 76: 9724–9734.
21. Hashizume C, Kuramitsu M, Zhang X, Kurosawa T, Kamata M, et al. (2007) Human immunodeficiency virus type 1 Vpr interacts with spliceosomal protein SAP145 to mediate cellular pre-mRNA splicing inhibition. Microbes Infect 9: 490–497.
22. Kuramitsu M, Hashizume C, Yamamoto N, Azuma A, Kamata M, et al. (2005) A novel role for Vpr of human immunodeficiency virus type 1 as a regulator of the splicing of cellular pre-mRNA. Microbes Infect 7: 1150–1160.
23. Roshal M, Zhu Y, Planelles V (2001) Apoptosis in AIDS. Apoptosis 6: 103–116.
24. Li G, Elder RT, Dubrovsky L, Liang D, Pushkarsky T, et al. (2010) HIV-1 replication through hHR23A-mediated interaction of Vpr with 26S proteasome. PLoS One 5: e11371.
25. Kamata M, Aida Y (2000) Two putative alpha-helical domains of human immunodeficiency virus type 1 Vpr mediate nuclear localization by at least two mechanisms. J Virol 74: 7179–7186.
26. Bukrinsky MI, Haffar OK (1998) HIV-1 nuclear import: matrix protein is back on center stage, this time together with Vpr. Mol Med 4: 138–143.
27. Fouchier RA, Meyer BE, Simon JH, Fischer U, Albright AV, et al. (1998) Interaction of the human immunodeficiency virus type 1 Vpr protein with the nuclear pore complex. J Virol 72: 6004–6013.
28. Le Rouzic E, Mousnier A, Rustum C, Stutz F, Hallberg E, et al. (2002) Docking of HIV-1 Vpr to the nuclear envelope is mediated by the interaction with the nucleoporin hCG1. J Biol Chem 277: 45091–45098.
29. Suzuki T, Yamamoto N, Nonaka M, Hashimoto Y, Matsuda G, et al. (2009) Inhibition of human immunodeficiency virus type 1 (HIV-1) nuclear import via Vpr-Importin alpha interactions as a novel HIV-1 therapy. Biochem Biophys Res Commun 380: 838–843.
30. Morellet N, Bouaziz S, Petitjean P, Roques BP (2003) NMR structure of the HIV-1 regulatory protein VPR. J Mol Biol 327: 215–227.
31. Romani B, Engelbrecht S (2009) Human immunodeficiency virus type 1 Vpr: functions and molecular interactions. J Gen Virol 90: 1795–1805.
32. Lum JJ, Cohen OJ, Nie Z, Weaver JG, Gomez TS, et al. (2003) Vpr R77Q is associated with long-term nonprogressive HIV infection and impaired induction of apoptosis. J Clin Invest 111: 1547–1554.
33. Nishizawa M, Myojin T, Nishino Y, Nakai Y, Kamata M, et al. (1999) A carboxy-terminally truncated form of the Vpr protein of human immunodeficiency virus type 1 retards cell proliferation independently of G(2) arrest of the cell cycle. Virology 263: 313–322.
34. Chen M, Elder RT, Yu M, O'Gorman MG, Selig L, et al. (1999) Mutational analysis of Vpr-induced G2 arrest, nuclear localization, and cell death in fission yeast. J Virol 73: 3236–3245.
35. Ao Z, Danappa Jayappa K, Wang B, Zheng Y, Kung S, et al. (2010) Importin {alpha}3 Interacts with HIV-1 Integrase and Contributes to HIV-1 Nuclear Import and Replication. J Virol 84: 8650–8663.
36. Wang P, Palese P, O'Neill RE (1997) The NPI-1/NPI-3 (karyopherin alpha) binding site on the influenza a virus nucleoprotein NP is a nonconventional nuclear localization signal. J Virol 71: 1850–1856.
37. Cook A, Fernandez E, Lindner D, Ebert J, Schlenstedt G, et al. (2005) The structure of the nuclear export receptor Cse1 in its cytosolic state reveals a closed conformation incompatible with cargo binding. Mol Cell 18: 355–367.
38. Sun C, Yang W, Tu LC, Musser SM (2008) Single-molecule measurements of importin alpha/cargo complex dissociation at the nuclear pore. Proc Natl Acad Sci U S A 105: 8613–8618.
39. Zhou Y, Lu Y, Ratner L (1998) Arginine residues in the C-terminus of HIV-1 Vpr are important for nuclear localization and cell cycle arrest. Virology 242: 414–424.
40. Jenkins Y, McEntee M, Weis K, Greene WC (1998) Characterization of HIV-1 vpr nuclear import: analysis of signals and pathways. J Cell Biol 143: 875–885.
41. Jacquot G, Le Rouzic E, David A, Mazzolini J, Bouchet J, et al. (2007) Localization of HIV-1 Vpr to the nuclear envelope: impact on Vpr functions and virus replication in macrophages. Retrovirology 4: 84.
42. Kobe B (1999) Autoinhibition by an internal nuclear localization signal revealed by the crystal structure of mammalian importin alpha. Nat Struct Biol 6: 388–397.
43. Agostini I, Popov S, Li J, Dubrovsky L, Hao T, et al. (2000) Heat-shock protein 70 can replace viral protein R of HIV-1 during nuclear import of the viral preintegration complex. Experimental cell research 259: 398–403.
44. Goodwin DJ, Whitehouse A (2001) A gamma-2 herpesvirus nucleocytoplasmic shuttle protein interacts with importin alpha 1 and alpha 5. J Biol Chem 276: 19905–19912.
45. Fagerlund R, Melen K, Kinnunen L, Julkunen I (2002) Arginine/lysine-rich nuclear localization signals mediate interactions between dimeric STATs and importin alpha 5. J Biol Chem 277: 30072–30078.
46. Melen K, Fagerlund R, Franke J, Kohler M, Kinnunen L, et al. (2003) Importin alpha nuclear localization signal binding sites for STAT1, STAT2, and influenza A virus nucleoprotein. J Biol Chem 278: 28193–28200.
47. Tarendeau F, Boudet J, Guilligay D, Mas PJ, Bougault CM, et al. (2007) Structure and nuclear import function of the C-terminal domain of influenza virus polymerase PB2 subunit. Nat Struct Mol Biol 14: 229–233.
48. Aida Y, Matsuda G (2009) Role of Vpr in HIV-1 nuclear import: therapeutic implications. Curr HIV Res 7: 136–143.
49. Herbein G, Varin A (2010) The macrophage in HIV-1 infection: from activation to deactivation? Retrovirology 7: 33.
50. Hagiwara K, Murakami T, Xue G, Shimizu Y, Takeda E, et al. (2010) Identification of a novel Vpr-binding compound that inhibits HIV-1 multiplication in macrophages by chemical array. Biochem Biophys Res Commun.
51. Nishino Y, Myojin T, Kamata M, Aida Y (1997) Human immunodeficiency virus type 1 Vpr gene product prevents cell proliferation on mouse NIH3T3 cells without the G2 arrest of the cell cycle. Biochem Biophys Res Commun 232: 550–554.
52. Kitayama H, Miura Y, Ando Y, Hoshino S, Ishizaka Y, et al. (2008) Human immunodeficiency virus type 1 Vpr inhibits axonal outgrowth through induction of mitochondrial dysfunction. J Virol 82: 2528–2542.

doi:10.1016/j.jmb.2011.04.061 J. Mol. Biol. (2011) 410, 887–895

Contents lists available at www.sciencedirect.com

Journal of Molecular Biology

journal homepage: http://ees.elsevier.com.jmb

COMMUNICATION

Functional Characterization of Human Cyclin T1 N-Terminal Region for Human Immunodeficiency Virus-1 Tat Transcriptional Activation

Kaori Asamitsu[1], Yurina Hibi[1], Kenichi Imai[1], Ann Florence B. Victoriano[1], Eiji Kurimoto[2], Koichi Kato[2] and Takashi Okamoto[1]*

[1]*Department of Molecular and Cellular Biology, Nagoya City University Graduate School for Medical Sciences, 1 Kawasumi, Mizuho-cho, Mizuho-ku, Nagoya, Aichi 467-8601, Japan*

[2]*Department of Structural Biology and Biomolecular Engineering, Graduate School of Pharmaceutical Sciences, Nagoya City University, 3-1 Tanabe-dori, Mizuho-ku, Nagoya 467-8603, Japan*

Received 1 April 2011; received in revised form 26 April 2011; accepted 26 April 2011

Edited by M. F. Summers

Keywords:
P-TEFb;
transcription;
HIV-1 LTR;
protein–protein interaction;
3D structure

Transcription of the human immunodeficiency virus type 1 (HIV-1) requires the interaction of the cyclin T1 (CycT1) subunit of a host cellular factor, positive transcription elongation factor b, with the viral Tat protein at the transactivation response (TAR) element of nascent viral transcripts. The involvement of the interaction between Tat and CycT1 is known to be through the Tat–TAR recognition motif (TRM) on CycT1. Here, we have further characterized this molecular interaction and clarified the role of the CycT1 N-terminal region in Tat action. We found crucial and distinctive roles of Q46, Q50 and F176 of human CycT1 protein in Tat-mediated transcription by creating various Ala substitution mutants of CycT1 based on its three-dimensional structure. We confirmed the involvement of these amino acid residues in binding to Tat with Q46 and Q50, and to a lesser extent with F176, by *in vitro* pull-down assay. Relative transactivation activities of wild-type CycT1 chimeras and mutant derivatives on the HIV-1 long terminal repeat were determined by luciferase reporter assays. Whereas CycT1 Q46A alone had impaired transcriptional activity, the CycT1(Q46A)–Tat chimeric protein retained almost full activity of the wild-type CycT1. However, CycT1 mutants (C261Y, Q50A or F176A) or their chimeric counterparts had lost the transactivation capacity. Moreover, a triple-mutant chimera containing Q46A, Q50A and F176A mutations completely abolished the transcriptional activity, indicating that these amino acid residues are involved through distinct mechanisms. These findings provide new insights for the development of anti-HIV drugs.

*Corresponding author. E-mail address: tokamoto@med.nagoya-cu.ac.jp.

Present address: E. Kurimoto, Faculty of Pharmacy, Meijo University, 150 Yagotoyama, Tempaku-ku, Nagoya 468-8503, Japan.

Abbreviations used: HIV-1, human immunodeficiency virus type 1; P-TEFb, positive transcription elongation factor b; CycT1, cyclin T1; CDK9, cyclin-dependent kinase 9; TAR, transactivation response element; aa, amino acids; TRM, Tat–TAR recognition motif; LTR, long terminal repeat; hCycT1, human CycT1; WT, wild type.

Introduction

Transcription of the human immunodeficiency virus type 1 (HIV-1) is a highly regulated process in which multiple cellular transcription factors and a single viral transactivator protein, Tat, are involved.[1–4] Tat stimulates transcriptional elongation from HIV-1 proviral DNA by mediating the positive transcription elongation factor b (P-TEFb) to the TAR element, an RNA stem–loop structure spontaneously formed at the 5′ end of all HIV-1 mRNA transcripts.[5] The active form of P-TEFb is composed of a regulatory subunit, cyclin T1 (CycT1), and a catalytic subunit, cyclin-dependent kinase 9 (CDK9).[6–8] CycT1 has been shown to be an essential cofactor of Tat and binds cooperatively with Tat to TAR RNA.[8,9] CDK9 phosphorylates the C-terminal domain of RNA polymerase II.[10–12] Thus, a current working model suggests that Tat recruits P-TEFb to the nascent viral transcripts, allowing CDK9 to hyperphosphorylate the polymerase II C-terminal domain and activate HIV-1 transcription at the step of elongation.

CycT1 contains 726 residues and a cyclin box domain (from positions 31 to 250), a coiled-coil sequence (from 379 to 530), and a PEST sequence (from positions 709 to 726).[12,13] The first 272 amino acids of CycT1 are sufficient to bind Tat and TAR and mediate Tat activation.[7] A region near the C-terminus of CycT1 1–272, termed the Tat–TAR recognition motif (TRM), is crucial for forming the Tat–CycT1–TAR ternary complex.[8] In the CycT1 TRM, the Cys residue at position 261 plays an essential role for its binding to Tat and TAR by forming a Zn^{2+}-dependent interaction with other Cys and His residues within Tat at positions 1 through 48.[6–8,14] Indeed, murine CycT1, whose Cys at position 261 is changed to Tyr, cannot support Tat action.[7,8,14]

Several studies have been conducted to analyze the functional relationships within the TAR–Tat–P-TEFb complex and Tat transcriptional activity. For example, CycT1 mutants whose crucial amino acid residues within TRM were substituted to Ala disrupted its interaction with Tat and/or TAR and abolished Tat action in augmenting HIV-1 transcription.[8] Besides TRM, other regions of CycT1 are essential for the Tat-mediated transactivation. The N-terminal cyclin box of CycT1 contributes to the Tat-mediated transcriptional regulation through binding to CDK9.[13,15] In addition, three Thr residues, T143, T149 and T155, in CycT1 were shown to be important for Tat action.[16] When all three Thr residues were substituted by Ala, although the formation of the Tat–TAR–P-TEFb complex was not hampered, the Tat-mediated transactivation was greatly diminished presumably through binding of negative regulators.[16] Furthermore, it was shown that the N-terminal region of CycT1 containing amino acids 67–71 was crucial for Tat transactivation. Deletion of this region resulted in the degradation of Tat.[17] Recently, the crystal structure of human P-TEFb (CycT1/CDK9) and the HIV-1 Tat complex has been resolved and provided structural information regarding the Tat–P-TEFb complex formation. Multiple hydrogen bonds were found between Tat and the N-terminal amino acid residues of CycT1.[18]

In this study, we have evaluated the effects of the N-terminal region of CycT1 in the Tat-mediated transcriptional activation of the HIV-1 long terminal repeat (LTR) and Tat–CycT1 protein–protein interaction *in vitro*. By Ala substitution mutagenesis of CycT1, we found that some amino acid residues exhibited essential roles in supporting Tat action.

Possible Involvement of the N-Terminal Region of CycT1 in Binding to Tat

As demonstrated in Fig. 1a, based on the three-dimensional (3D) structure of human CycT1 (hCycT1) protein reported by Anand *et al.*,[19] there is a deep cleft consisting of the N-terminal amino acid residues between 26 and 53 and the known interacting surface called "TRM" with HIV-1 Tat. We examined whether this cleft held by TRM (amino acids 250–263) and this N-terminal region (amino acids 26–53) could stably interact with Tat and is involved in the Tat-mediated transcriptional activation of HIV-1 LTR. As shown in Fig. 1b, the extent to which various CycT1 mutants supported Tat-mediated transcriptional activation was compared in murine NIH3T3 cells, where endogenous CycT1 does not support Tat action. When the N-terminal 49 amino acid (aa) residues were deleted, Tat-mediated transactivation was greatly suppressed [compare "WT" (lane 3) and "50–278" (lane 4)]. Even a slight dominant-negative effect of exogenous mutant CycT1 was observed (compare lanes 2 and 4). We then constructed a series of mutant CycT1 wherein the amino acid side chains facing the abovementioned Tat-interacting cleft, namely, R26, D30, D32, K33, L35, S36, Y37, Q39, Q40, N43, Q46, D47, Q50 and N53, were substituted with Ala and examined their effects on HIV-1 LTR gene expression mediated by Tat. Among these mutants, CycT1(Q46A) and CycT1(Q50A) lost the ability to support the Tat action. In addition, since two other amino acids at F176 and H183 residues appeared to be involved in forming the Tat-interacting cleft, these were also substituted (Fig. 1c). We found that CycT1(F176A) and CycT1 (H183A) mutants showed complete and partial loss of such activity, respectively. Consistent with a previous observation,[8] the CycT1 TRM mutants, R251A, C261Y and C261A, had impaired transactivation activity (Fig. 1d). These results with CycT1

mutants could not be ascribed to the decreased protein stability because the steady-state levels of mutant CycT1 proteins did not exhibit significant change (Fig. 1e). In Fig. 1f, we have similarly examined the effects of full-length hCycT1 and its mutants bearing Ala substitution at the indicated amino acid residues on the Tat-mediated transactivation. Results were fully consistent with those obtained using CycT1 described above. Significant inhibition of Tat-mediated transactivation was evident with mutants Q46A, Q50A, F176A, C261Y and C261A. Thus, the C-terminal truncation of CycT1 does not appear to change the action of CycT1 as previously reported.[7,8]

Interaction between Tat and Various CycT1 Mutants *in Vitro*

To further determine whether these CycT1 amino acid residues are involved in the interaction with Tat, recombinant His-tagged CycT1 proteins were constructed, expressed in bacteria and purified. As shown in Fig. 2a, similar amounts of recombinant CycT1 proteins were recovered to near homogeneity. These proteins did not exhibit significant changes in 3D structure as demonstrated by circular dichroism (CD) spectrum analysis (Fig. 2b). Thus, we performed an *in vitro* pull-down assay using GST (glutathione *S*-transferase)–Tat fusion protein and various His-tagged hCycT1 proteins (Fig. 2c). Results showed that wild-type CycT1(WT) and other functional CycT1 mutants (Q40A and D47A) physically interacted with Tat, while three CycT1 mutants (Q46A, Q50A and C261Y) had lost their ability to bind Tat. Although CycT1 mutant D47A did not impair Tat transactivation, a slight decrease in Tat binding was observed. Ala substitution of CycT1(F176) that conforms a hydrophobic patch between CycT1 and Tat[18] significantly disrupted transactivation function without affecting Tat binding. It was noted that the Tat binding of CycT1 (C261Y) mutant was impaired at the first 15 min; however, this protein–protein binding was observed by 30 min, suggesting the involvement of other Tat-interacting amino acids in its binding to compensate for the C261Y mutation.

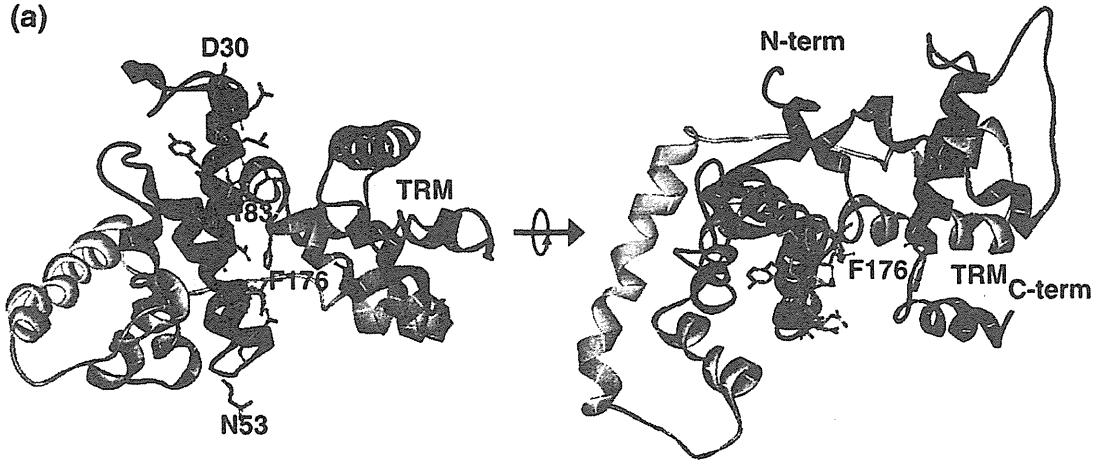

Fig. 1. Involvement of the N-terminal region of hCycT1 in binding to Tat. (a) 3D structure of CycT1. The rotated figure is shown in the right panel. This hCycT1 structure was taken from the crystallographic representation of the Tat–hCycT1 fusion protein reported in Anand *et al.* (2pk2_a).[19] CycT1 TRM (250–263 aa) and N-terminal helix (30–53 aa) are depicted in red and blue, respectively. Within the N-terminal helix, those amino acid residues whose amino acid side chains are facing toward TRM are depicted in yellow. (b–d) Various hCycT1 mutants and their effects on the Tat-mediated HIV-1 transactivation. These CycT1(1–278) mutants were created by Ala substitution mutagenesis, and their ability to support Tat-mediated HIV-1 LTR transactivation in murine NIH3T3 cells was examined. Details for plasmid construction are described in the supplemental information. The relative luciferase (reporter gene) activity, in "fold" activation, was compared. The luciferase expression plasmid under the transcriptional control of HIV-1 LTR, CD12-luc (containing the HIV-1 LTR U3 and R), was previously described.[20] All the experiments were conducted in triplicates, and the data were presented as the fold increase in luciferase activities (mean ± SD) relative to the control of three independent transfections. (e) Expression of wild-type (WT) and mutant CycT1 proteins in HEK293 (human embryonic kidney 293) cells. hCycT1-expressing plasmid DNA (200 ng) was transfected into 293 cells using Fugene-6™ reagent. Forty-eight hours later, cells were harvested and equal amounts of protein from cell lysates were separated by SDS-PAGE. Protein expression level was determined by Western blotting using anti-FLAG antibody (Sigma) or antibody to human β-tubulin (Santa Cruz Biotechnology). (f) Various full-length hCycT1 mutants and their activities in the Tat-mediated HIV-1 transactivation.

Transcriptional Activity of the CycT1–Tat Chimera Proteins

Fujinaga *et al.*[21] previously demonstrated that the CycT1 N-terminal region (amino acids 1–59) was crucial to support Tat-mediated transactivation using CycT1–Tat chimeric proteins in NIH3T3 cells. Apart from introducing single point mutations of those amino acids that were found earlier to exhibit defective phenotype (Figs. 1 and 2) in CycT1, we also synthesized double-mutant CycT1–Tat fusion protein, and both were examined for their effects on Tat action, using murine cells (Fig. 3). As shown in Fig. 3b, the relative activities of these

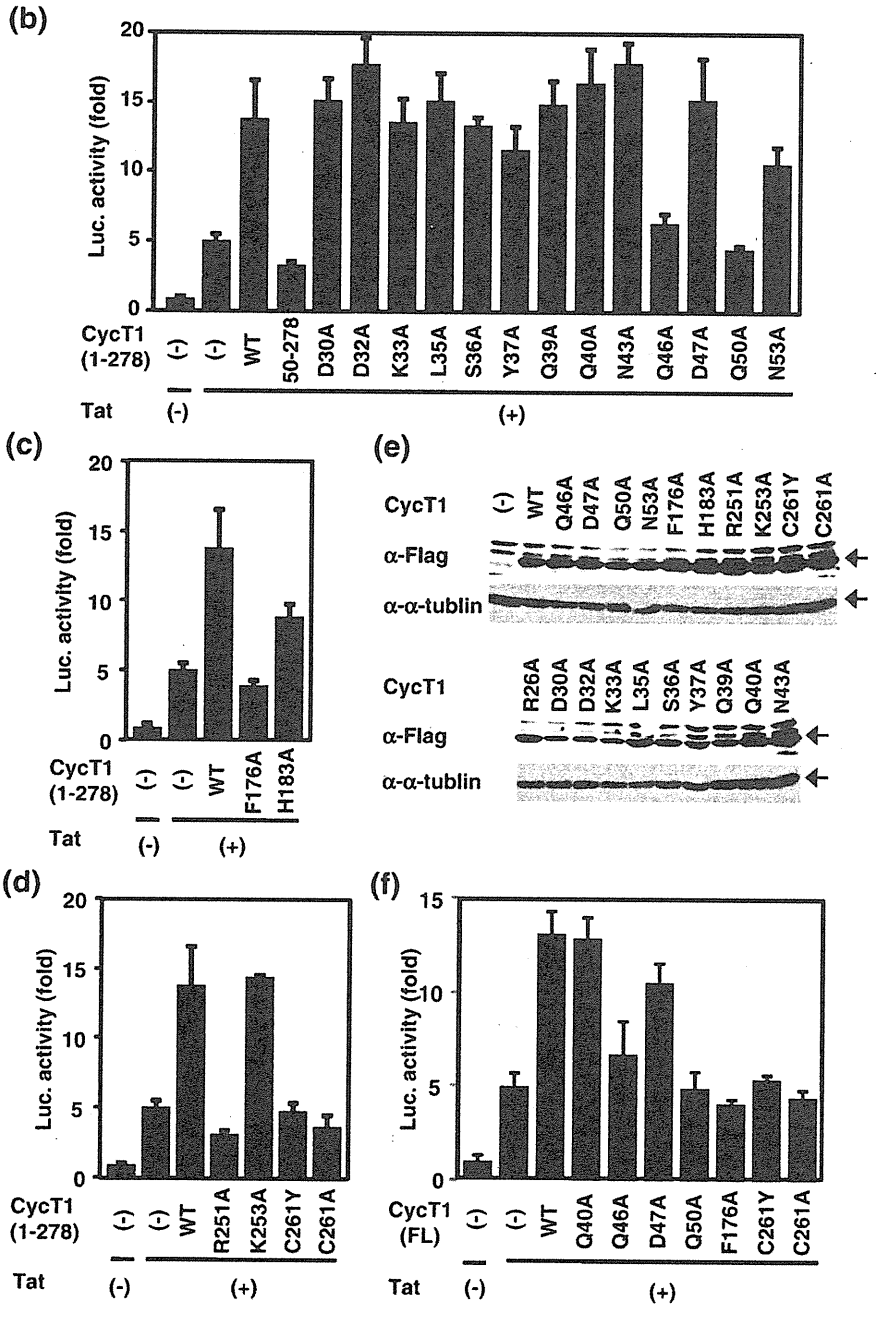

Fig. 1 *(legend on previous page)*

chimeras to activate HIV-1 LTR transcription were comparable with those of their nonchimeric counterparts (Fig. 1b–d and f); however, more remarkable effects were observed with the latter. The activity of CycT1–Tat WT was abolished when C261 was substituted by Tyr in accordance with previous findings,[8,21] indicating that the CycT1 portion of the fusion protein binds Tat and TAR in cells. The C261Y mutation in CycT1 greatly abolished the Tat-mediated transactivation, since C261 of CycT1 is known to be involved in its binding to TAR as well as to Tat. CycT1–Tat mutants Q46A, Q50A and F176A showed partial loss of transcriptional activity, whereas the Q40A mutant exhibited full transcriptional activity, and D47A exhibited a little higher activity. Although we do not currently have a reasonable explanation for this observation, it is possible that CycT1–Tat fusion protein might exhibit a little different transcriptional activity in some cases.

These results were largely consistent with earlier cotransfection experiments (Fig. 1), although Q46A mutation conferred a less remarkable effect on the CycT1(Q46A)–Tat fusion protein. Meanwhile, the double mutant [CycT1(Q46A, Q50A)–Tat] with Ala substitutions at both positions 46 and 50 exhibited a more pronounced defect in transactivation assay than the single mutant CycT1(Q46A) or CycT1 (Q50A)–Tat, which suggests that Q46 may cooperate with Q50 in modulating Tat action. We then created a triple chimeric mutant, CycT1(Q46A, Q50A, F176A)–Tat, and found that this mutant completely abolished the transcriptional activity of Tat and its effect was almost equivalent to that of the C261Y mutant. These results indicate that CycT1 amino acids Q46, Q50, F176 and C261 are involved in Tat-mediated transcriptional regulation through distinct mechanisms. In other words, either Q46 and Q50 or C261 is required for the CycT1 interaction with Tat, presumably independently, and F176 is involved together with Q46 and Q50. Since the transcriptional activity of CycT1(C261A) and CycT1(F176A) was substantially reduced without a complete loss of binding to Tat, amino acid residues such as C261A and F176A might also be involved in the recognition of TAR.

It is crucial for HIV-1 Tat to physically interact with relevant CycT1 to exert its action as the HIV-1-specific transcriptional activator.[1–4] Although a

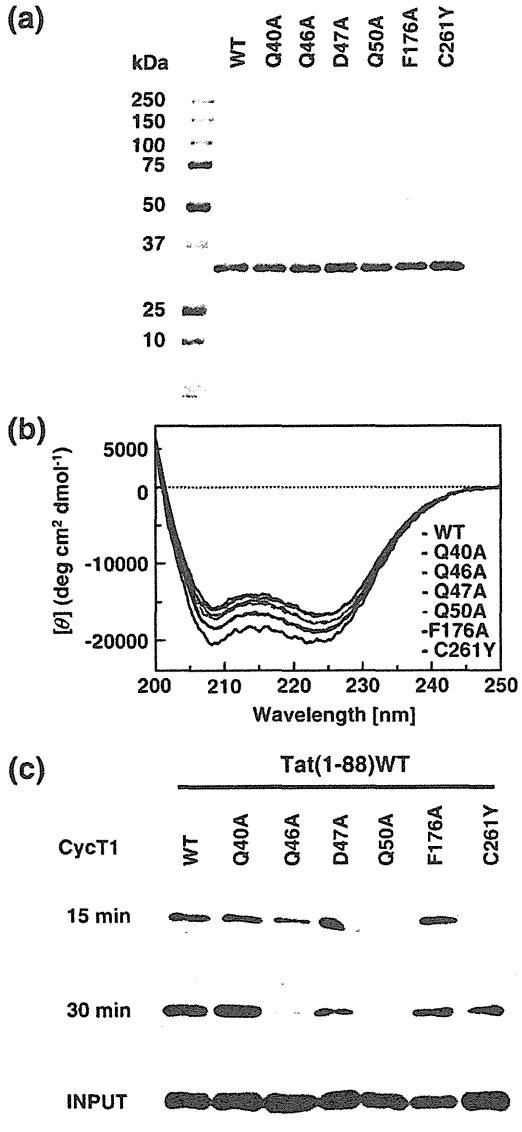

Fig. 2. Detection of protein–protein interaction between Tat and various hCycT1 proteins *in vitro*. (a) Purification of recombinant hCycT1. Recombinant hCycT1 proteins were affinity-purified using a nickel chelate column (GE Healthcare) according to the manufacture's protocol. Equal amounts of hCycT1 proteins were separated by SDS-PAGE and the gel was stained by Coomassie brilliant blue. The expected size (34 kDa) of recombinant hCycT1 protein is indicated by an arrowhead. (b) CD spectrum of the purified hCycT1 protein. CD spectra in the 200- to 250-nm region were measured for various CycT1 samples at 0.087–0.132 mg/ml in phosphate-buffered saline (pH 7.4) using a J-725 spectropolarimeter (JASCO) at 20 °C. After substraction of the spectrum of the buffer alone, data were represented as mean residue ellipticities. (c) *In vitro* pull-down assay between Tat and hCycT1. The His-tagged hCycT1 protein (12 μg) was incubated with 12 μg of GST–Tat fusion protein prebound to glutathione *S*-Sepharose beads (10 μl) in 500 μl of binding buffer [20 mM Hepes (pH 7.9), 0.5% NP-40, 1% Triton X, 0.7% β-mercaptoethanol, 0.1% bovine serum albumin and 0.7% $ZnCl_2$] containing 200 mM KCl. Incubations were carried out for 15 and 30 min at 4 °C. Beads were washed three times with binding buffer containing 1 M KCl, and eluted fractions were applied to 15% SDS-PAGE and then Western blotted with antibody against His tag.

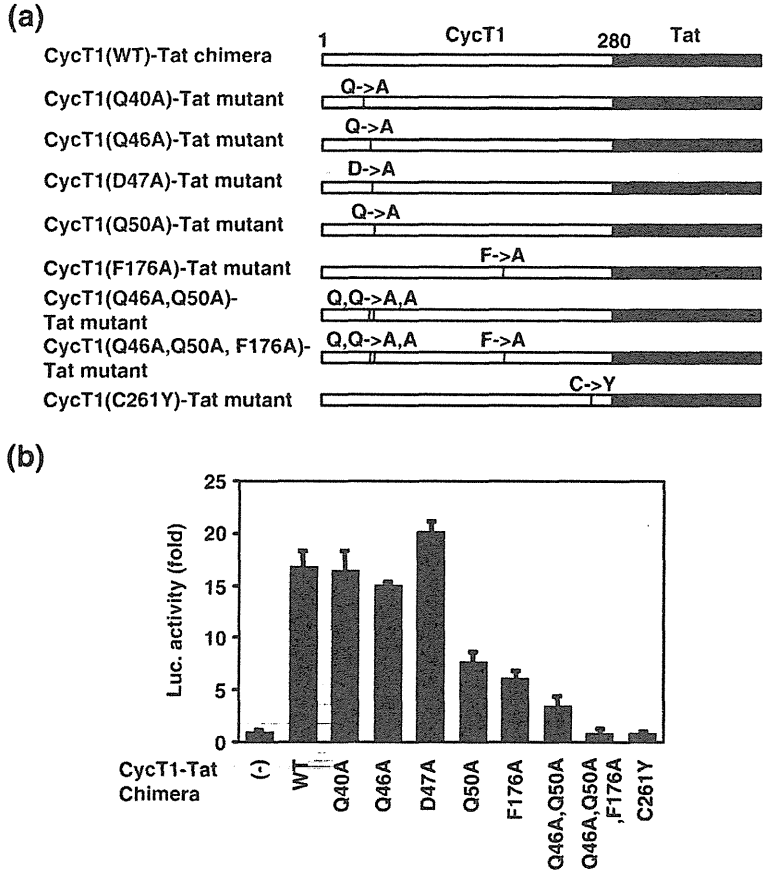

Fig. 3. Analysis of the transactivation properties of CycT1 and Tat chimeras. (a) Schematic representation of hCycT1(1–280) WT and mutant fusion proteins used in this study. (b) Transactivation activities of WT and mutant CycT1–Tat chimeras on the HIV-1 LTR. The plasmid expressing the hCycT1 and Tat chimera was reported in Fujinaga *et al.*[21] Plasmid construction and luciferase assay were carried out as described in Fig. 1b.

number of previous studies have deciphered several essential amino acid residues that participate in the Tat–CycT1 and CycT1–TAR interaction, most of these studies were based on random or targeted amino acid mutagenesis, and the CycT1 amino acid mutagenesis based on the structural model of the complex has not been reported.

In this study, we have identified CycT1 amino acid residues involved in its interaction with Tat and thus essential for its function. We found that not only the previously known TRM but also the N-terminal region of CycT1 is crucial for Tat function. Although the deletion of the CycT1 N-terminus was reported to abolish Tat activity, site-directed amino acid mutagenesis has not been carried out because of the lack of data showing the CycT1–Tat contact at the atomic level. However, a recent report by Anand *et al.*[22] showing a 3D structure of a fusion protein of Tat from equine infectious anemia virus (EIAV) and hCycT1 presented the detailed CycT1 structure and revealed that the TRM and the N-terminal regions of CycT1 make a molecular cleft that would fit the Tat protein, thus prompting us to pursue this study. We confirmed the involvement of some amino acid residues of the CycT1 N-terminus predicted to be facing toward the inside of this molecular cleft in Tat-mediated HIV-1 transcriptional activation and found that their respective contributions to transactivation were affected when the Tat moiety was artificially fused to CycT1 (compare Figs. 1 and 3). For example, whereas CycT1(Q46A) resulted in significant reduction in mediating Tat transactivation, the CycT1(Q46A)–Tat fusion chimera retained full transcriptional activity. In addition, C261Y CycT1 mutation abolished the Tat action on HIV-1 LTR; however, its potential to interact with Tat was partially restored. CycT1 mutants Q46A and Q50A both lost their ability to support Tat transactivation and interact with Tat. Meanwhile, their respective Tat chimeric proteins did not completely lose their transactivation potential. These findings suggest that these two amino acids might be primarily involved in the interaction between CycT1 and Tat. Two other CycT1 mutants, C261A and F176A, which failed to support Tat transactivation by itself or when fused with Tat, lost the Tat-supporting activity in luciferase gene expression assays even in forms of fusion proteins with Tat that failed to mediate Tat transactivation by itself or when fused with Tat, might be involved in the interaction with another molecule such as TAR. A recent crystallographic analysis of the Tat–CycT1–CDK9 complex

by Tahirov *et al.*[18] clearly indicated the involvement of F176 in the interaction with Tat.

Two recent papers have contributed the structural biological analyses of Tat–TAR–P-TEFb(CycT1).[18,22] Anand *et al.*[22] showed that EIAV Tat is bent around the first cyclin box repeat of CycT1, and H79, R80 and Tyr37 of CycT1 were crucial for recognition of Tat and TAR molecules and thus are involved in the formation of the Tat–TAR–CycT1 trimolecular complex. Moreover, using HIV-1 Tat, Tahirov *et al.*[18] have revealed the crystal structure of Tat–P-TEFb (CycT1 and CDK9) and demonstrated that the Tat 3D structure is complementary to the surface of P-TEFb and makes extensive contacts with the CycT1 subunit of P-TEFb. Interestingly, we have demonstrated that F176A mutation caused a significant decrease in the Tat-mediated transcriptional activation when CycT1 and Tat were transduced separately. However, since the Tat-binding activity of CycT1(F176A) mutant was still evident, although its binding affinity was diminished, it is possible that CycT1 F176 is also involved in the interaction with other essential molecules such as TAR RNA.

Furthermore, Tahirov *et al.*[18] also claim that Tat interacts with CycT1 through additional amino acids, namely, Q40, N43, D47, R51, N53, V54, Q97, Q172, D180 and D250, by forming numerous direct and water-mediated hydrogen bonds. However, mutations at some of these amino acids including Q40, N43, and D47 did not exhibit significant reduction of the Tat-mediated transactivation. These findings suggest that regulation of the Tat-mediated transcriptional activation of HIV-1 may also involve another mechanisms such as modulation of Tat stability[23] and its association with negative factors.[16]

Although the RXL motif in most of the CDK/cyclin substrates such as p24 and p21 is known to play a key role,[24,25] and the target Arg is recognized by Glu on the first helix of cyclin A, the interaction between CycT1 and Tat appears to use a distinct amino acid interaction. However, Tahirov *et al.*[18] showed that Asp (D) at amino acid 47 of CycT1 binds to Tyr (Y) at amino acid 47 of Tat. Since this region of Tat protein is conserved among distinct HIV-1 isolates, this interaction may represent a novel interaction. Moreover, since Tat does not contain the consensus RXL motif and the Tat–CycT1 interaction does not appear to depend on the presence of CDK9,[12,13] the interaction between these two molecules, Tat and CycT1, is considered crucial for the Tat-mediated transactivation.

Anti-HIV-1 drugs with inhibitory activity against Tat action can be classified into two categories with respect to their modes of action: (i) inhibition of Tat and TAR binding and (ii) inhibition of P-TEFb activity.[26–28] In the past two decades, several independent groups have identified small chemicals and peptide mimetic ligands for TAR.[29–33] However, none had sufficient therapeutic potency and specificity that warrant further pharmaceutical development. Several approaches have been undertaken to block HIV-1 transcription by targeting P-TEFb using small chemical compounds or mutant proteins that inhibit CDK9 kinase activity or disrupt the interaction between Tat, TAR and CycT1.[34–37] Since P-TEFb is involved in transcription of many cellular genes, structural target of specific anti-Tat compounds should exclude P-TEFb protein surfaces deemed to be critical for the interaction with cellular transcription factors. It is crucially important to elucidate the Tat-specific CycT1 molecular surface for the development of an efficient and yet specific anti-HIV reagent. Thus, our findings described here should facilitate the molecular design of compounds that would selectively inhibit Tat-dependent activation of P-TEFb and specifically block HIV-1 replication.

Supplementary materials related to this article can be found online at doi:10.1016/j.jmb.2011.04.061

Acknowledgements

We thank Dr. Ko Fujinaga for kindly providing the expression plasmid for CycT1–Tat fusion protein, pLINK–CycT1–Tat, and Mr. Yusuke Kobayashi for technical assistance. This study is supported in part by grants-in-aid from the Ministry of Health, Labor and Welfare of Japan and the Ministry of Education, Culture, Sports, Science and Technology of Japan.

References

1. Karn, J. (1999). Tackling Tat. *J. Mol. Biol.* **293**, 235–254.
2. Taube, R., Fujinaga, K., Wimmer, J., Barboric, M. & Peterlin, B. M. (1999). Tat transactivation: a model for the regulation of eukaryotic transcriptional elongation. *Virology*, **264**, 245–253.
3. Mancebo, H. S., Lee, G., Flygare, J., Tomassini, J., Luu, P., Zhu, Y. *et al.* (1997). P-TEFb kinase is required for HIV Tat transcriptional activation in vivo and in vitro. *Genes Dev.* **11**, 2633–2644.
4. Zhu, Y., Pe'ery, T., Peng, J., Ramanathan, Y., Marshall, N., Marshall, T. *et al.* (1997). Transcription elongation factor P-TEFb is required for HIV-1 Tat transactivation in vitro. *Genes Dev.* **11**, 2622–2632.
5. Peterlin, B. M. & Price, D. H. (2006). Controlling the elongation phase of transcription with P-TEFb. *Mol. Cell*, **23**, 297–305.
6. Bieniasz, P. D., Grdina, T. A., Bogerd, H. P. & Cullen, B. R. (1998). Recruitment of a protein complex

containing Tat and cyclin T1 to TAR governs the species specificity of HIV-1 Tat. *EMBO J.* **17**, 7056–7065.
7. Fujinaga, K., Taube, R., Wimmer, J., Cujec, T. P. & Peterlin, B. M. (1999). Interactions between human cyclin T, Tat, and the transactivation response element (TAR) are disrupted by a cysteine to tyrosine substitution found in mouse cyclin T. *Proc. Natl Acad. Sci. USA*, **96**, 1285–1290.
8. Garber, M. E., Wei, P., KewalRamani, V. N., Mayall, T. P., Herrmann, C. H., Rice, A. P. *et al.* (1998). The interaction between HIV-1 Tat and human cyclin T1 requires zinc and a critical cysteine residue that is not conserved in the murine CycT1 protein. *Genes Dev.* **12**, 3512–3527.
9. Garber, M. E., Wei, P. & Jones, K. A. (1998). HIV-1 Tat interacts with cyclin T1 to direct the P-TEFb CTD kinase complex to TAR RNA. *Cold Spring Harb. Symp. Quant. Biol.* **63**, 371–380.
10. Fu, T. J., Peng, J., Lee, G., Price, D. H. & Flores, O. (1999). Cyclin K functions as a CDK9 regulatory subunit and participates in RNA polymerase II transcription. *J. Biol. Chem.* **274**, 34527–34530.
11. Marshall, N. F., Peng, J., Xie, Z. & Price, D. H. (1996). Control of RNA polymerase II elongation potential by a novel carboxyl-terminal domain kinase. *J. Biol. Chem.* **271**, 27176–27183.
12. Peng, J., Zhu, Y., Milton, J. T. & Price, D. H. (1998). Identification of multiple cyclin subunits of human P-TEFb. *Genes Dev.* **12**, 755–762.
13. Wei, P., Garber, M. E., Fang, S. M., Fischer, W. H. & Jones, K. A. (1998). A novel CDK9-associated C-type cyclin interacts directly with HIV-1 Tat and mediates its high-affinity, loop-specific binding to TAR RNA. *Cell*, **92**, 451–462.
14. Ivanov, D., Kwak, Y. T., Nee, E., Guo, J., Garcia-Martinez, L. F. & Gaynor, R. B. (1999). Cyclin T1 domains involved in complex formation with tat and TAR RNA are critical for *tat*-activation. *J. Mol. Biol.* **288**, 41–56.
15. Fujinaga, K., Irwin, D., Geyer, M. & Peterlin, B. M. (2002). Optimized chimeras between kinase-inactive mutant Cdk9 and truncated cyclin T1 proteins efficiently inhibit Tat transactivation and human immunodeficiency virus gene expression. *J. Virol.* **76**, 10873–10881.
16. Jadlowsky, J. K., Nojima, M., Okamoto, T. & Fujinaga, K. (2008). Dominant negative mutant cyclin T1 proteins that inhibit HIV transcription by forming a kinase inactive complex with Tat. *J. Gen. Virol.* **89**, 2783–2787.
17. Jadlowsky, J. K., Nojima, M., Schulte, A., Geyer, M., Okamoto, T. & Fujinaga, K. (2008). Dominant negative mutant cyclin T1 proteins inhibit HIV transcription by specifically degrading Tat. *Retrovirology*, **5**, 63.
18. Tahirov, T. H., Babayeva, N. D., Varzavand, K., Cooper, J. J., Sedore, S. C. & Price, D. H. (2010). Crystal structure of HIV-1 Tat complexed with human P-TEFb. *Nature*, **465**, 747–751.
19. Anand, K., Schulte, A., Fujinaga, K., Scheffzek, K. & Geyer, M. (2007). Cyclin box structure of the P-TEFb subunit cyclin T1 derived from a fusion complex with EIAV tat. *J. Mol. Biol.* **370**, 826–836.
20. Takada, N., Sanda, T., Okamoto, H., Yang, J. P., Asamitsu, K., Sarol, L. *et al.* (2002). RelA-associated inhibitor blocks transcription of human immunodeficiency virus type 1 by inhibiting NF-κB and Sp1 actions. *J. Virol.* **76**, 8019–8030.
21. Fujinaga, K., Irwin, D., Taube, R., Zhang, F., Geyer, M. & Peterlin, B. M. (2002). A minimal chimera of human cyclin T1 and Tat binds TAR and activates human immunodeficiency virus transcription in murine cells. *J. Virol.* **76**, 12934–12939.
22. Anand, K., Schulte, A., Vogel-Bachmayr, K., Scheffzek, K. & Geyer, M. (2008). Structural insights into the cyclin T1–Tat–TAR RNA transcription activation complex from EIAV. *Nat. Struct. Mol. Biol.* **15**, 1287–1292.
23. Imai, K., Asamitsu, K., Victoriano, A. F., Cueno, M. E., Fujinaga, K. & Okamoto, T. (2009). Cyclin T1 stabilizes expression levels of HIV-1 Tat in cells. *FEBS J.* **276**, 7124–7133.
24. Brown, N. R., Noble, M. E., Endicott, J. A. & Johnson, L. N. (1999). The structural basis for specificity of substrate and recruitment peptides for cyclin-dependent kinases. *Nat. Cell. Biol.* **1**, 438–443.
25. Wohlschlegel, J. A., Dwyer, B. T., Takeda, D. Y. & Dutta, A. (2001). Mutational analysis of the Cy motif from p21 reveals sequence degeneracy and specificity for different cyclin-dependent kinases. *Mol. Cell. Biol.* **21**, 4868–4874.
26. Richter, S. N. & Palu, G. (2006). Inhibitors of HIV-1 Tat-mediated transactivation. *Curr. Med. Chem.* **13**, 1305–1315.
27. Baba, M. (2006). Recent status of HIV-1 gene expression inhibitors. *Antiviral. Res.* **71**, 301–306.
28. Stevens, M., De Clercq, E. & Balzarini, J. (2006). The regulation of HIV-1 transcription: molecular targets for chemotherapeutic intervention. *Med. Res. Rev.* **26**, 595–625.
29. Hwang, S., Tamilarasu, N., Kibler, K., Cao, H., Ali, A., Ping, Y. H. *et al.* (2003). Discovery of a small molecule Tat-*trans*-activation-responsive RNA antagonist that potently inhibits human immunodeficiency virus-1 replication. *J. Biol. Chem.* **278**, 39092–39103.
30. Hamy, F., Felder, E. R., Heizmann, G., Lazdins, J., Aboul-ela, F., Varani, G. *et al.* (1997). An inhibitor of the Tat/TAR RNA interaction that effectively suppresses HIV-1 replication. *Proc. Natl Acad. Sci. USA*, **94**, 3548–3553.
31. Afshar, M., Prescott, C. D. & Varani, G. (1999). Structure-based and combinatorial search for new RNA-binding drugs. *Curr. Opin. Biotechnol.* **10**, 59–63.
32. Murchie, A. I., Davis, B., Isel, C., Afshar, M., Drysdale, M. J., Bower, J. *et al.* (2004). Structure-based drug design targeting an inactive RNA conformation: exploiting the flexibility of HIV-1 TAR RNA. *J. Mol. Biol.* **336**, 625–638.
33. Mayer, M., Lang, P. T., Gerber, S., Madrid, P. B., Pinto, I. G., Guy, R. K. & James, T. L. (2006). Synthesis and testing of a focused phenothiazine library for binding to HIV-1 TAR RNA. *Chem. Biol.* **13**, 993–1000.
34. Okamoto, H., Cujec, T. P., Okamoto, M., Peterlin, B. M., Baba, M. & Okamoto, T. (2000). Inhibition of the RNA-dependent transactivation and replication of

human immunodeficiency virus type 1 by a fluoroquinoline derivative K-37. *Virology*, **272**, 402–408.
35. Chao, S. H. & Price, D. H. (2001). Flavopiridol inactivates P-TEFb and blocks most RNA polymerase II transcription *in vivo*. *J. Biol. Chem.* **276**, 31793–31799.
36. Chao, S. H., Fujinaga, K., Marion, J. E., Taube, R., Sausville, E. A., Senderowicz, A. M. *et al.* (2000). Flavopiridol inhibits P-TEFb and blocks HIV-1 replication. *J. Biol. Chem.* **275**, 28345–28348.
37. Wang, X., Yamataka, K., Okamoto, M., Ikeda, S. & Baba, M. (2007). Potent and selective inhibition of Tat-dependent HIV-1 replication in chronically infected cells by a novel naphthalene derivative JTK-101. *Antivir. Chem. Chemother.* **18**, 201–211.

nature
structural &
molecular biology

The APOBEC3C crystal structure and the interface for HIV-1 Vif binding

Shingo Kitamura[1,2], Hirotaka Ode[1], Masaaki Nakashima[1,2], Mayumi Imahashi[1,3], Yuriko Naganawa[1], Teppei Kurosawa[1,2], Yoshiyuki Yokomaku[1], Takashi Yamane[2], Nobuhisa Watanabe[2,4], Atsuo Suzuki[2], Wataru Sugiura[1,3] & Yasumasa Iwatani[1,3]

The human apolipoprotein B mRNA-editing enzyme catalytic polypeptide–like 3 (APOBEC3, referred to as A3) proteins are cellular cytidine deaminases that potently restrict retrovirus replication. However, HIV-1 viral infectivity factor (Vif) counteracts the antiviral activity of most A3 proteins by targeting them for proteasomal degradation. To date, the structure of an A3 protein containing a Vif-binding interface has not been solved. Here, we report a high-resolution crystal structure of APOBEC3C and identify the HIV-1 Vif–interaction interface. Extensive structure-guided mutagenesis revealed the role of a shallow cavity composed of hydrophobic or negatively charged residues between the α2 and α3 helices. This region is distant from the DPD motif (residues 128–130) of APOBEC3G that participates in HIV-1 Vif interaction. These findings provide insight into Vif-A3 interactions and could lead to the development of new pharmacologic anti–HIV-1 compounds.

The A3 family of cytidine deaminases consists of cellular proteins that prevent the mobilization of diverse retroviruses, retrotransposons and other viral pathogens (reviewed in ref. 1). In humans, seven members of this protein family, A3A, A3B, A3C, A3DE, A3F, A3G and A3H, are encoded in a tandem array on chromosome 22 (ref. 2). The A3 proteins are characterized by the presence of one or two conserved zinc-coordinating domains (Z domains) consisting of $HXE(X)_{23-28}CXXC$ motifs (reviewed in ref. 3). On the basis of phylogenetic analyses, the Z domains fall into three types: Z1 (A3A and the C-terminal domains (CTDs) of A3B and A3G), Z2 (A3C, both halves of A3DE and A3F, and the N-terminal domains (NTDs) of A3B and A3G) and Z3 (A3H)[2]. The Z2 domain can be further subdivided into three subgroups on the basis of amino acid sequences: the A3F NTD (the NTDs of A3B, A3DE and A3F), the A3G NTD and the A3F CTD (A3C and the CTDs of A3DE and A3F) subgroups.

HIV-1 Vif protein overcomes the antiviral activity of A3 proteins in infected cells by forming an E3 ubiquitin ligase complex, with cullin 5, elongin B (EloB) and elongin C (EloC) in collaboration with core-binding factor β (CBF-β)[4,5], which subsequently leads to A3 degradation through the ubiquitin-proteasome pathway[6–8]. Thus, the elimination of A3 in cells during virus production prevents its encapsidation into progeny HIV-1 viruses. A3 degradation specificity is determined by the ability of Vif to bind to the target. HIV-1 Vif binds A3C, A3DE, A3F, A3G and A3H but not A3A and A3B. Among the Z domains, only Z3 (A3H haplotype II) and Z2 (the A3G NTD and the A3F CTD subgroups) contain a critical interface that interacts with HIV-1 Vif[9–11].

One specific residue of the human A3G NTD responsible for the Vif interaction, Asp128, was primarily identified by comparative studies of species-specific A3G-Vif interactions[12–15]. Subsequently, extensive mutational analyses of amino acids adjacent to Asp128 revealed that the 128-Asp-Pro-Asp-130 (DPD) motif of A3G, located at loop 7 between β4 and α4, is crucial for the direct interaction with Vif[16]. These critical residues in the A3G NTD have been mapped to a variable-loop structure in close proximity to the nucleic acid–binding surface. In contrast, two independent studies have reported that two residues that are critical for the Vif interaction, Glu289 and Glu324 of the A3F CTD, are situated in the α3 and α4 helices, respectively, which are located distally from the DPD motif[10,17]. Despite our knowledge of these critical A3 residues, the structural features underlying the Vif-interaction interface on A3 proteins have not been previously elucidated.

To date, the three-dimensional structure of only the A3G CTD has been determined by NMR[18,19] or X-ray crystallography[20,21]. The structures of full-length A3 or the domain involved in the HIV-1 Vif–binding interface have not been previously solved. Here, we present the first report, to our knowledge, of the crystal structure of full-length human A3C. We used extensive structure-guided mutagenesis to explore the residues that form the HIV-1 Vif–binding interface. Our results demonstrate that ten residues of A3C are critical for the formation of the Vif-interaction interface, which mapped to a different region from loop 7 that corresponds to an area of the DPD motif in the A3G NTD. Furthermore, our data indicate that the responsible interface provides a shallow cavity composed of hydrophobic or

[1]Clinical Research Center, Department of Infectious Diseases and Immunology, National Hospital Organization Nagoya Medical Center, Nagoya, Japan. [2]Department of Biotechnology, Graduate School of Engineering, Nagoya University, Nagoya, Japan. [3]Program in Integrated Molecular Medicine, Graduate School of Medicine, Nagoya University, Nagoya, Japan. [4]Synchrotron Radiation Research Center, Nagoya University, Nagoya, Japan. Correspondence should be addressed to Y.I. (iwataniy@nnh.hosp.go.jp).

Received 23 April; accepted 7 August; published online 23 September 2012; doi:10.1038/nsmb.2378

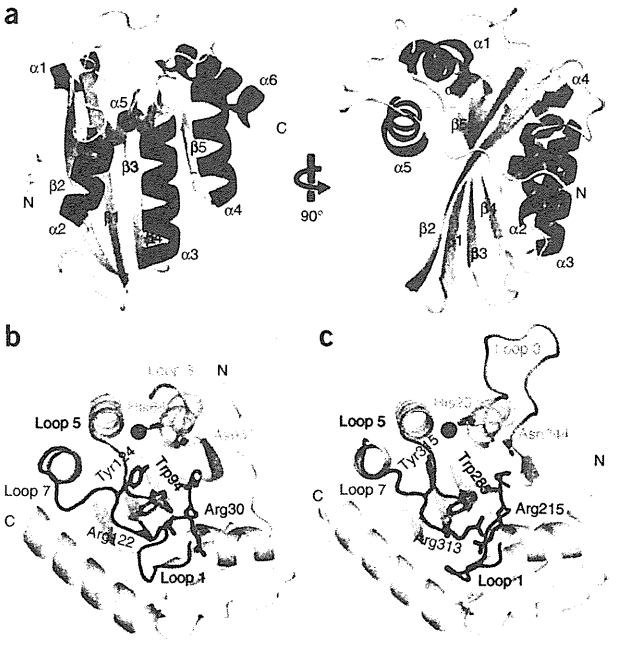

Figure 1 The X-ray crystal structure of full-length A3C. (**a**) Two views of the A3C structure, rotated by 90°, are shown. The α-helices (α1–α6) and β-strands (β1–β5) are colored in red and yellow, respectively. A coordinated zinc ion is represented as a blue sphere. (**b**,**c**) Structural comparison around the catalytic groove of A3C (**b**) and A3G CTD (**c**). Amino acid side chains of the conserved residues in loop 1 (magenta), loop 3 (yellow), loop 5 (orange) and loop 7 (cyan) are labeled with the residue numbers.

negatively charged residues. In addition, we found that the structural features of the Vif-binding interfaces are conserved in the homologous Z2-type A3C, A3F and A3DE proteins but not in the A3G protein. These results will deepen our understanding of A3-Vif interactions and aid in the development of new strategies using potential endogenous inhibitors against HIV-1.

RESULTS

High-resolution crystal structure of full-length A3C

Initially, human A3C was expressed in *Escherichia coli* as an N-terminal GST-tagged recombinant protein to increase its solubility. The tag was subsequently removed. We further purified the full-length A3C protein (residues 1–190) and solved its structure at 2.15 Å (**Fig. 1a** and **Table 1**). The A3C structure has a core platform composed of six α-helices (α1–α6) and five β-strands (β1–β5), with a coordinated zinc ion that is well conserved in the cytidine deaminase superfamily[22]. The superimposition of the A3C core onto that of the A3G CTD crystal structure (PDB 3IR2) for 86% of the backbone atoms exhibited a Cα r.m.s. deviation of 1.36 Å, thereby indicating the structural conservation of the core platform.

In contrast to the high conservation of the core structures, the loop regions, particularly loops 1, 3, 4 and 7 of the A3C and A3G CTD structures, are distinct (**Fig. 1b,c** and **Supplementary Fig. 1a,b**). Nevertheless, the positions of certain residues in the loops exhibit structural similarity. Arg30, Asn57, His66, Trp94, Arg122 and Tyr124 in A3C (**Fig. 1b**) are similar to Arg215, Asn244, His257, Trp285, Arg313 and Tyr315 in the A3G CTD (**Fig. 1c**). These residues primarily have critical roles in maintaining the conformation of the catalytic center and the groove involved in substrate binding[18,20], which are functionally conserved features among A3 proteins. In contrast, differences in the HIV-1 Vif interaction are attributable to unique conformational differences between the A3C and A3G CTD structures.

Notably, the A3C structure exhibits a continuous well-ordered β2-strand that is remarkably different from that of the A3G CTD (PDB 3IR2) (**Fig. 1** and **Supplementary Fig. 1a,b**). Molecular dynamics (MD) simulations support the high stability of the A3C β2 (**Supplementary Fig. 1c–f**), which is also observed in the APOBEC2 (A2) crystal structure[23]. In the A2 structure, a continuous β2 strand mediates dimerization through a β2 of another molecule. However, we did not detect any intermolecular contacts through the β2-β2 interaction within the 20 largest contacts in the crystal packing (**Supplementary Fig. 2a**). In addition, our dynamic light-scattering experiments indicated both monomodal and bimodal distributions of A3C proteins in solution (**Supplementary Fig. 2b**), although our gel-filtration data indicated that most of the protein was distributed in the monomer size fraction (**Supplementary Fig. 2c**). These results suggest that dynamic A3C dimerization might occur but not through their β2 strands. This effect might be partly owing to 13 amino acids of the N-terminal region, which reside on the β2 strand, that sterically hinder the β2-β2 associations. Recently, a similar observation with a full-length A2 structure has also been reported[24].

Ten A3C residues are critical for HIV-1 Vif binding

To determine the interface for HIV-1 Vif recognition of A3C, extensive structure-guided mutagenesis experiments were performed by using an approach analogous to that previously described for A3G[25]. A single

Table 1 Data collection and refinement statistics

	APOBEC3C
Data collection	
Space group	$P6_1$
Cell dimensions	
a, *b*, *c* (Å)	105.04, 105.04, 70.05
α, β, γ (°)	90, 90, 120
Resolution (Å)	105–2.15 (2.19–2.15)
R_{merge}	5.4 (33.8)
$I / \sigma I$	94.5 (13.3)
Completeness (%)	99.9 (100)
Redundancy	22.3 (22.6)
Refinement	
Resolution (Å)	91–2.15
No. reflections	22,783
R_{work} / R_{free}	21.4 / 26.3
No. atoms	3,281
Protein	3,188
Ligand/ion	3
Water	90
B factors	45.56
Protein	45.69
Ligand/ion	45.50
Water	40.90
R.m.s. deviations	
Bond lengths (Å)	0.012
Bond angles (°)	1.390

A single crystal was used for solving the structure. Values in parentheses are for highest-resolution shell.

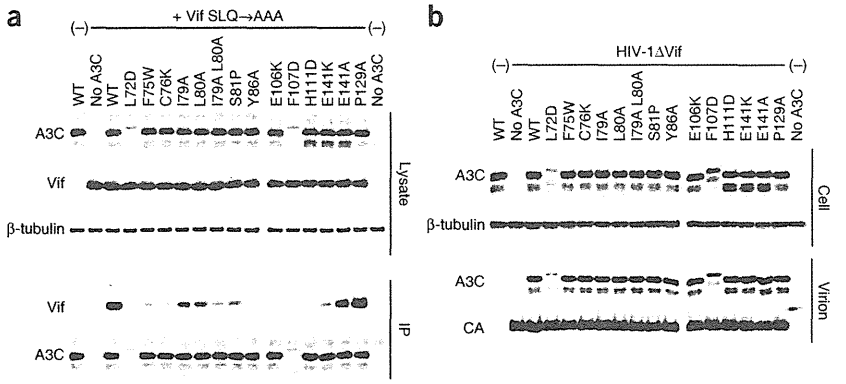

Figure 2 Ten A3C residues critical for HIV-1 Vif interaction. (**a**) Immunoblots of lysates and anti-His immunoprecipitates of HEK-293T cells with wild type (WT), mutant A3C-Myc-His or control plasmid (no A3C) expressed in the presence (+) or absence (–) of HIV-1 Vif SLQ→AAA. Immunoblotting is with anti-Vif or anti-His monoclonal antibodies as shown. Anti–β-tubulin antibody was used as a loading control. IP, immunoprecipitation. (**b**) Virion-packaging efficiency of Vif-resistant A3C mutants. Intracellular (cell) and virus-incorporated (virion) levels of A3C WT and mutants analyzed by western blotting. Samples are from cells transfected with HIV-1ΔVif or control plasmids (–), plus either A3C or control plasmids (no A3C). The HIV-1 capsid protein (CA) levels in virions were detected with an anti-p24 antibody.

E106K substitution changes the susceptibility of A3C to Vif-mediated degradation[10], which suggests that Glu106 is one of the residues responsible for the A3C-Vif interaction. Therefore, to further identify the other critical residues adjacent to Glu106, we first introduced substitution mutations near Glu106 and tested the Vif sensitivity *in vitro*. The results are summarized in **Supplementary Figure 3**. Wild-type A3C was not detectable when coexpressed with Vif (Vif sensitive), whereas the expression of the E106K mutant was unchanged in the presence of Vif (Vif resistant). These experiments were repeated for all residues whose mutations resulted in a Vif-resistant phenotype, until the surrounding A3C surface residues were all associated with sensitive mutants. The percentage reduction of A3C expression in the presence relative to the absence of Vif was evaluated (Vif-resistance level) (**Supplementary Fig. 3**). The results indicated that any single point mutation in the nine residues (Leu72, Phe75, Cys76, Ile79, Leu80, Ser81, Tyr86, Glu106 and Phe107) resulted in a >50% Vif-resistance level, whereas the mutations H111D and A109K resulted in 45% and 41% resistance, respectively. To evaluate whether these residues were intrinsically involved in the Vif interaction, we immunoprecipitated a Vif SOCS-box mutant (Vif SLQ→AAA) that can bind A3 but not EloBC[8,26,27] in the presence of wild-type or Myc-His-tagged A3C mutants, and immunoblotted for Vif SLQ→AAA (**Fig. 2a**). Vif was coimmunoprecipitated with wild-type A3C and A3C P129A at equal levels (**Fig. 2a**), which indicated that Pro129 in A3C is not responsible for the Vif interaction, unlike findings with A3G[16]. In contrast, all of the Vif-resistant A3C mutants immunoprecipitated minimal amounts of Vif, which indicated that the residues whose mutations conferred the Vif-resistant phenotypes are indeed critical for the Vif interaction. The E141K mutation abolished Vif binding, despite being relatively Vif sensitive. The reason for this effect is not clear. These findings demonstrated that Leu72, Phe75, Cys76, Ile79, Leu80, Ser81, Tyr86, Glu106, Phe107 and His111 are involved in forming the Vif-interaction interface. All of the binding-deficient A3C mutants were incorporated into *vif*-deficient HIV-1 (HIV-1ΔVif) as efficiently as wild-type A3C (**Fig. 2b**), which suggested that RNA-binding capacity was not impaired by the A3C mutations.

Structural mapping of the mutagenesis results yielded a Vif-resistance level, which is color-coded on the structure (**Fig. 3a,b**). The residues involved in the Vif interaction are located in an area between the α2 and α3 helices, distal from the Pro129 of the A3G DPD motif[16]. Notably, in the A3C surface representation, the interface is a shallow cavity composed of hydrophobic (Leu72, Ile79 and Leu80) or aromatic (Phe75, Tyr86, Phe107 and His111) residues at the bottom and hydrophilic (Cys76, Ser81 and Glu106) residues at the edges (**Fig. 3a–c**). One notable feature of this cavity is that two potential π interactions can be observed at the bottom, on the basis of the configuration of four aromatic residues (Phe75, Tyr86, Phe107

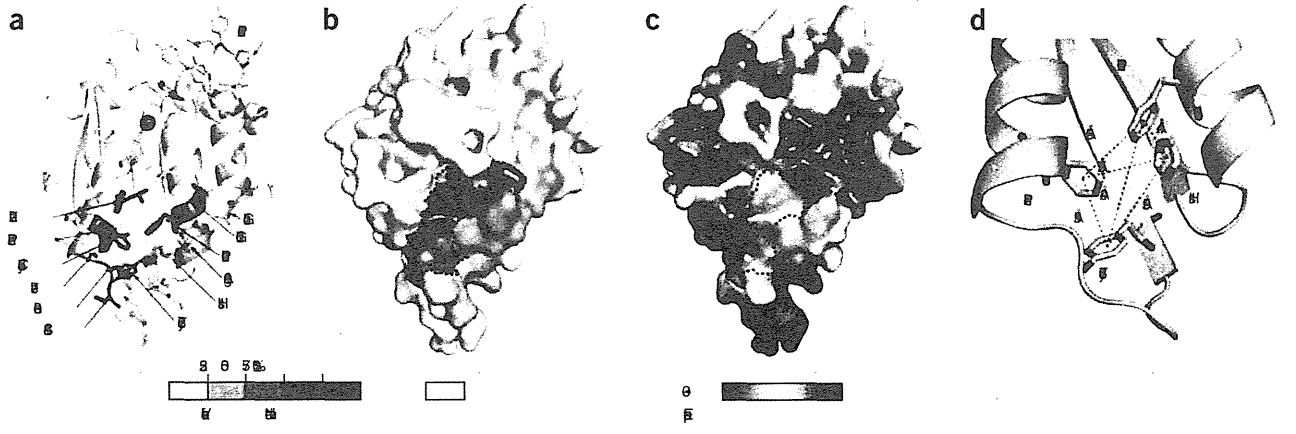

Figure 3 The A3C interface for the HIV-1 Vif interaction. (**a**,**b**) The A3C structure, displaying critical residues for Vif sensitivity. The residues are colored in the ribbon (**a**) and surface (**b**) representations of A3C according to the resistance level of Vif-mediated degradation, as shown in the bottom bar. Residues exhibiting a >50% Vif-resistance level are enclosed by a dotted line. (**c**) The electrostatic potential of A3C is shown. The accessible surface area is colored according to the calculated electrostatic potential from –3 *kT/e* (red) to 3 *kT/e* (blue). The orientation and the dotted line are the same as in **b**. (**d**) Potential π-stacking interactions at the Vif-binding interface in A3C. The distances between the four aromatic residues involved in the Vif-binding cavity (Phe75, Tyr86, Phe107 and His111) are shown.

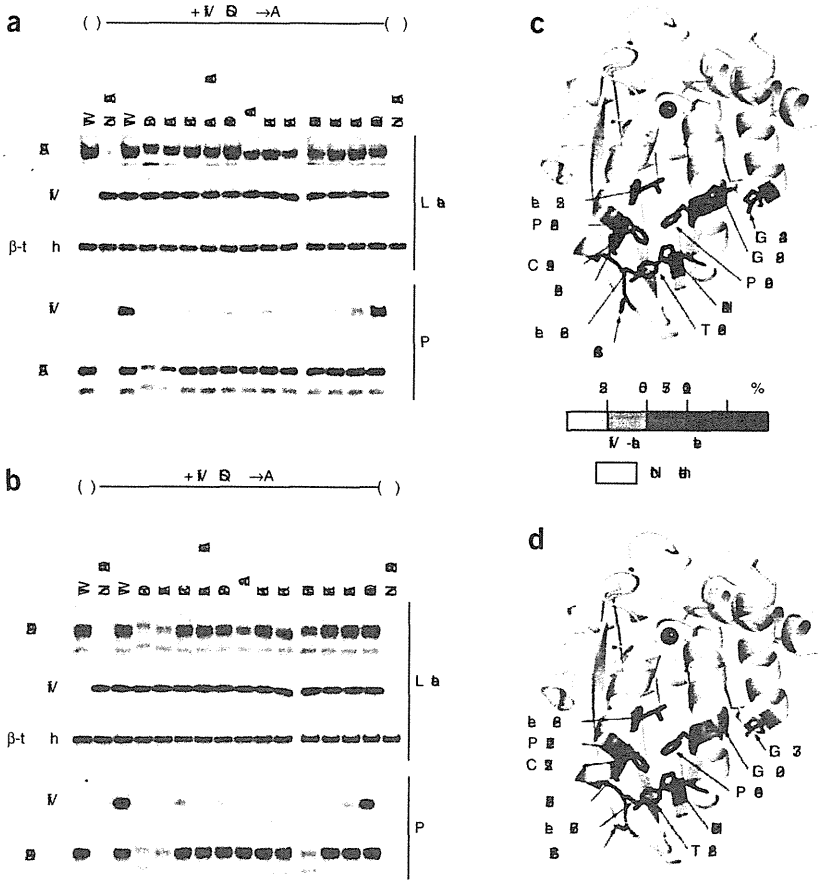

Figure 4 Analogous residues of A3F and A3DE are involved in the HIV-1 Vif-binding interface. (**a**,**b**) Coimmunoprecipitation (IP) of HIV-1 Vif SLQ→AAA with wild type (WT) or A3F-MycHIS mutants (**a**) and with wild type or A3DE-MycHIS mutants (**b**). (**c**,**d**) Residues are mapped on the A3F (**c**) or the A3DE CTD (**d**) structures modeled on the A3C crystal structure. The residues are color coded according to their Vif-resistance levels. A coordinated zinc ion is shown as a blue sphere.

and His111) (**Fig. 3d**). Both Phe75-Tyr86 and Phe107-His111 show the proper distance and orientation to make two weak π-π interactions. In contrast, the pair of Phe75-Phe107 shows theoretically proper distance, although the angle is not appropriate to form a potential interaction. In addition, because a mutation of the hydrophobic or aromatic residues disrupts the Vif interaction and subsequent degradation, a specific size of the hydrophobic side chains, as well as π stacking, may be important for maintaining the correct interface conformation and for the A3C-Vif interaction. The interface includes a flexible region, loop 4, where Cys76, Ile79, Leu80 and Ser81 exhibit higher temperature factors in the crystal-structure data and in the MD simulations (**Supplementary Fig. 1f**), which suggests a partially flexible interface. Furthermore, the electrostatic surface potential analysis revealed a negatively charged interface (**Fig. 3c**), and substitutions with positively charged residues increase the Vif-resistance levels (**Supplementary Fig. 3**), which suggests that the negative electrostatic surface at the interface is also an important feature for HIV-1 Vif binding.

Vif-binding interfaces are conserved in A3C, A3F and A3DE

We also performed analogous coimmunoprecipitation experiments with equivalent mutations in the A3F and A3DE CTDs and tested for Vif interaction (**Fig. 4**). For A3F, involvement of the A3F Glu289 and Glu324 residues in Vif interaction has been reported[10,17]. Coimmunoprecipitates of these A3F mutants contained significantly reduced amounts of Vif (**Fig. 4a**) compared to wild type or E251Q (a mutation at the catalytic center), which demonstrates that the equivalent residues of A3F, Leu255, Phe258, Cys259, Ile262, Leu263, Ser264, Tyr269, Glu289, Phe290 and His294, are also important for the Vif interaction. In addition, we assessed the Vif sensitivity of the mutants (**Supplementary Fig. 3c,e**) and mapped the residues onto a homology model of the A3F CTD (**Fig. 4c**). Again, these residues were clustered and formed a Vif-binding cavity homologous to that observed in the A3C structure, although a slight difference in the Vif-resistant phenotype was observed. The E141K A3C mutant displayed a low Vif-resistance level (27%), whereas the corresponding A3F mutant, E324K, had a high resistance level (87%) (**Supplementary Fig. 3c,e**). MD simulations suggested that conformational differences at the negatively charged edge of the cavity may be responsible for these differences (**Supplementary Fig. 4**).

For A3DE, the analysis of the coimmunoprecipitation assays demonstrated that 10 equivalent residues (Leu268, Phe271, Cys272, Ile275, Leu276, Ser277, Tyr282, Glu302, Phe303 and His307) of A3DE are also important for Vif interaction (**Fig. 4b**). In addition, mutations at any of the residues critical for Vif interaction resulted in a Vif-resistant phenotype, although the A3DE S277D and E302K mutants presented a lower of the Vif-resistance than the equivalents of A3F S264D and E289K, respectively (**Supplementary Fig. 3c–f**). Moreover, these residues provide a similar Vif-binding interface to that of A3C (**Fig. 4d**). These results suggest that the conformation of the Vif-interaction interface is highly conserved among A3C and the CTDs of A3F and A3DE.

To further assess whether the Z2-type A3G NTD provides a similar Vif-interaction interface at the equivalent position between the α2 and α3 helices, we constructed four analogous A3G mutants, F74W, L80D, Y86A and F107K, that have a substitution at identical residues, on the basis of sequence alignments between A3C and the A3G NTD. Examination of Vif sensitivity in these mutants indicated that none of these mutations in the A3G NTD changed the Vif-sensitive phenotype (**Supplementary Fig. 5**). These results demonstrated that the Vif-binding interface of A3G NTD is distinct from that of A3C, A3F and A3DE. In addition, they suggest that mutations between the α2 and α3 helices do not distort the presumed Vif-binding interface conformation of the A3G NTD.

Vif-resistant A3F inhibits HIV-1 infection

To elucidate the effects of the A3F mutations on viral incorporation, we analyzed the amounts of wild-type and mutant A3F proteins in cells and virions. Both wild-type and mutant A3F were efficiently incorporated into virus particles, with the exception of the H294D

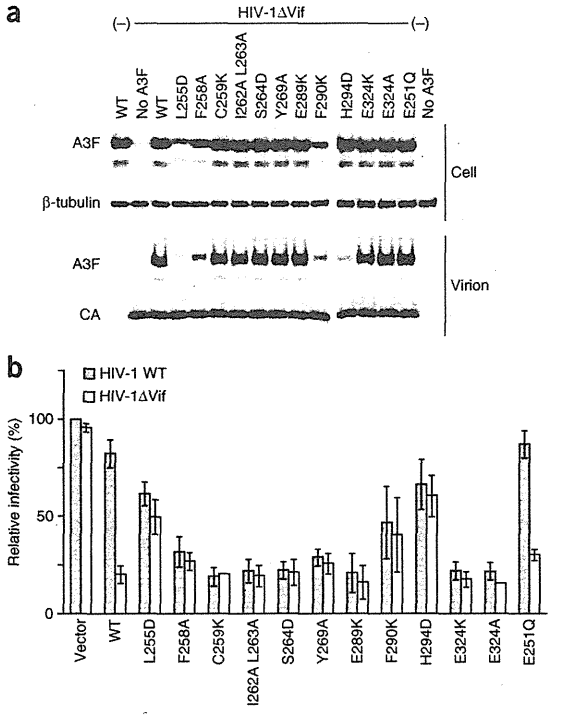

Figure 5 The effects of mutations at the equivalent residues in A3F on antiviral activity. (**a**) Intracellular expression (cell) and incorporation of wild-type A3F and the mutants into virions (virion), evaluated by western blotting. The CA level in virions was detected by an anti-p24 antibody. (**b**) The antiviral effects of A3F and mutants on wild-type HIV-1 (HIV-1 WT) or HIV-1ΔVif in a single-round replication assay with LuSIV cells. The relative viral infectivity of wild-type HIV-1 in the absence of A3F (vector) was set to 100%. Relative infectivity data are shown as means ± s.d. of three independent experiments.

mutant (**Fig. 5a**). This result suggests that the critical residues for Vif interaction (except for His294) of A3F are not located in the region that is responsible for A3F packaging into virions. Finally, to evaluate whether the A3F mutants exhibited any antiviral activity against HIV-1, we compared the infectivity of wild-type HIV-1 and HIV-1ΔVif in the presence of wild-type or mutant A3F. The wild-type A3F and the E251Q mutant reduced HIV-1ΔVif infectivity to 21% and 30%, respectively, whereas wild-type HIV-1 infectivity was only marginally affected (**Fig. 5b**). In contrast, all of the Vif-resistant A3F mutants suppressed the infectivity of wild-type HIV-1 as efficiently as for HIV-1ΔVif, which is consistent with their packaging level (**Fig. 5a,b**). These findings demonstrate that a disruption of the A3F-Vif interaction prevents A3F degradation and thereby allows A3F to be efficiently packaged into HIV-1 virions to exert its antiviral activity.

DISCUSSION

Studies conducted over the past decade have established that HIV-1 Vif abolishes the antiviral activity of A3 by recruiting an E3 ubiquitin ligase complex to promote proteasomal degradation. Many efforts toward developing strategies that interfere with the A3-Vif interaction have been unsuccessful to date, in part because of the lack of available structural information on the A3-Vif interaction interface. Here, we present, to our knowledge, the first crystal structure of A3C containing an HIV-1 Vif-interaction interface. In addition, our extensive structure-guided mutagenesis revealed the precise Vif-interaction site, between the α2 and α3 helices of A3C, and permitted the delineation of structural features (negatively charged, hydrophobic and partially flexible) in the Vif-interaction interface. Additional investigations demonstrated that the Vif-binding interfaces are highly conserved among Z2-type cytidine deaminases, including A3C, A3F and A3DE, but not A3G.

In combination with the A3C structure, our results suggest that the Vif-interaction interface forms a shallow cavity that is composed of hydrophobic and negatively charged residues. Notably, the positively charged DRMR motif (residues 14–17)[26] and hydrophobic residues (Leu24, Val25, Leu64, Ile66 and Leu72) on HIV-1 Vif are required for its specific interaction with A3C (reviewed in ref. 28), thereby confirming that both the electrostatic and hydrophobic interactions are the fundamental driving force for the A3C-Vif interaction. In addition, Vif Trp5, Trp21, Trp38, Tyr69, Trp70 and Trp89 are commonly considered essential for the interaction with A3C, A3F, A3DE or A3G. These data suggest that the π interactions of the aromatic residues between the A3C interface and Vif may contribute to their association, and these interactions are presumably common to all A3-Vif interactions. Recent reports indicate that Vif Trp21 and Trp38 are important for binding with the cofactor CBF-β. The π interactions may be mediated by CBF-β for efficient formation of the E3 ubiquitin ligase complex[4,5,29]. In addition, the existence of a partially flexible region in the Vif-binding interface (**Supplementary Fig. 1f**) suggests that the cavity may not locally exhibit a fixed conformation, and certain structural changes may be induced by Vif to allow a tight interaction.

Although the A3G NTD is categorized as a Z2-type cytidine deaminase, the amino acid sequences of the A3G NTD and A3C are quite different; only 42.8% of the A3C sequences are identical to the A3G NTD, whereas 77% and 76% are identical to the A3F CTD and A3DE CTD sequences, respectively. In particular, the residues of the α2–α3 regions are not homologous between A3C, A3F, A3DE and the A3G NTD, which suggests differences in their local conformations. For A3C, the Vif-binding interface is located in a region distal to loop 7 that corresponds to an area of the DPD motif in the A3G NTD. In addition, our homologous mutagenesis showed that the equivalent area of the A3G NTD between the α2 and α3 helices is not critical for the A3G-Vif interaction (**Supplementary Fig. 5**), demonstrating that two different regions in A3C and the A3G NTD molecules participate in each specific interaction with Vif. The presence of these distinct interfaces is consistent with the evidence that the HIV-1 Vif residues responsible for binding to A3 proteins are different. The YRHHY motif (residues 40–44) and the DRMR motif in Vif are involved in specific interactions with A3G, and A3C, A3F or A3DE, respectively[11,26,30–33]. Nevertheless, because both types of A3-Vif interactions fundamentally require electrostatic and hydrophobic bindings and the involvement of the flexible loop conformations (loop 4 for A3C, A3F or A3DE; loop 7 for A3G), the interfaces of A3C, A3F or A3DE and A3G may have similar structural characteristics.

Our determination of the high-resolution A3C crystal structure and extensive structure-guided mutagenesis revealed the A3C structural features associated with the Vif interaction. In addition, the conformation of the Vif-binding interface is highly conserved within the Z2-type A3 subfamily. The location of the Vif-binding interface on A3 proteins may prove to be important during the development of pharmacologic agents that target A3-Vif interactions. Previous reports have shown that the residues of A3G and A3C that are critical for nucleic acid binding also have essential roles in the efficient packaging

of A3 into virions[16,34]. These residues are involved in the formation of nucleic acid–binding grooves primarily consisting of loops 1, 3, 5 and 7 near the coordinated zinc ions of A3G and A3C proteins. The A3G DPD motif for Vif interaction is immediately adjacent to the four YYFW residues (124–127) necessary for A3G incorporation into virions[16]. Therefore, we must use caution to not perturb the contributions of the neighboring YYFW residues that are necessary for A3G incorporation into virions. In contrast, the Vif-binding interfaces that we identified in A3C, A3F and A3DE are mapped to a position distal to the nucleic acid–binding pocket that is important for A3's encapsidation into virions. Therefore, during drug discovery and development, it could be advantageous to target the interaction of Vif with A3C, A3F or A3DE, particularly that with A3F, without disturbing the nucleic acid–binding capability. Taken together, these findings on the structural features of Vif-binding interfaces may aid in our understanding of Vif-A3 interactions and lead to the development of new pharmacologic anti-HIV-1 compounds that could restore the activity of the intrinsic antiviral factor in the context of HIV-1 infection.

METHODS

Methods and any associated references are available in the online version of the paper.

Accession codes. Coordinates and structure factors have been deposited into the Protein Data Bank, with the accession code 3VOW.

Note: Supplementary information is available in the online version of the paper.

ACKNOWLEDGMENTS

We thank A.M. Gronenborn, J.G. Levin and K. Strebel for critical discussions and reading of the manuscript. We also thank K. Tokunaga (National Institute of Infectious Diseases, Tokyo, Japan) for providing the pCAGGS APOBEC3 plasmids. This work was supported in part by a grant from the Ministry of Education, Culture, Sports, Science and Technology of Japan to Y.I. (JSPS KAKENHI 24590568) and by a grant for HIV/AIDS research from the Ministry of Health, Labor and Welfare of Japan to Y.I.

AUTHOR CONTRIBUTIONS

S.K., H.O., M.N., T.K., T.Y., N.W., A.S. and Y.I. performed experiments and analysis for the crystal structure determination; S.K., M.N., M.I., Y.N., T.K., Y.Y. and Y.I. performed biochemical experiments; S.K., M.N., M.I., Y.N., Y.Y., W.S. and Y.I. analyzed the biochemical data; Y.I. directed the project; S.K., H.O. and Y.I. wrote the manuscript with all authors' help.

COMPETING FINANCIAL INTERESTS

The authors declare no competing financial interests.

Published online at http://www.nature.com/doifinder/10.1038/nsmb.2378.
Reprints and permissions information is available online at http://www.nature.com/reprints/index.html.

1. Goila-Gaur, R. & Strebel, K. HIV-1 Vif, APOBEC, and intrinsic immunity. *Retrovirology* **5**, 51 (2008).
2. LaRue, R.S. *et al.* Guidelines for naming nonprimate APOBEC3 genes and proteins. *J. Virol.* **83**, 494–497 (2009).
3. Wedekind, J.E., Dance, G.S., Sowden, M.P. & Smith, H.C. Messenger RNA editing in mammals: new members of the APOBEC family seeking roles in the family business. *Trends Genet.* **19**, 207–216 (2003).
4. Jäger, S. *et al.* Vif hijacks CBF-β to degrade APOBEC3G and promote HIV-1 infection. *Nature* **481**, 371–375 (2012).
5. Zhang, W., Du, J., Evans, S.L., Yu, Y. & Yu, X.F. T-cell differentiation factor CBF-β regulates HIV-1 Vif-mediated evasion of host restriction. *Nature* **481**, 376–379 (2012).
6. Marin, M., Rose, K.M., Kozak, S.L. & Kabat, D. HIV-1 Vif protein binds the editing enzyme APOBEC3G and induces its degradation. *Nat. Med.* **9**, 1398–1403 (2003).
7. Sheehy, A.M., Gaddis, N.C. & Malim, M.H. The antiretroviral enzyme APOBEC3G is degraded by the proteasome in response to HIV-1 Vif. *Nat. Med.* **9**, 1404–1407 (2003).
8. Yu, X. *et al.* Induction of APOBEC3G ubiquitination and degradation by an HIV-1 Vif-Cul5-SCF complex. *Science* **302**, 1056–1060 (2003).
9. Russell, R.A., Smith, J., Barr, R., Bhattacharyya, D. & Pathak, V.K. Distinct domains within APOBEC3G and APOBEC3F interact with separate regions of human immunodeficiency virus type 1 Vif. *J. Virol.* **83**, 1992–2003 (2009).
10. Smith, J.L. & Pathak, V.K. Identification of specific determinants of human APOBEC3F, APOBEC3C, and APOBEC3DE and African green monkey APOBEC3F that interact with HIV-1 Vif. *J. Virol.* **84**, 12599–12608 (2010).
11. Zhen, A., Wang, T., Zhao, K., Xiong, Y. & Yu, X.F. A single amino acid difference in human APOBEC3H variants determines HIV-1 Vif sensitivity. *J. Virol.* **84**, 1902–1911 (2010).
12. Bogerd, H.P., Doehle, B.P., Wiegand, H.L. & Cullen, B.R. A single amino acid difference in the host APOBEC3G protein controls the primate species specificity of HIV type 1 virion infectivity factor. *Proc. Natl. Acad. Sci. USA* **101**, 3770–3774 (2004).
13. Mangeat, B., Turelli, P., Liao, S. & Trono, D. A single amino acid determinant governs the species-specific sensitivity of APOBEC3G to Vif action. *J. Biol. Chem.* **279**, 14481–14483 (2004).
14. Schröfelbauer, B., Chen, D. & Landau, N.R. A single amino acid of APOBEC3G controls its species-specific interaction with virion infectivity factor (Vif). *Proc. Natl. Acad. Sci. USA* **101**, 3927–3932 (2004).
15. Xu, H. *et al.* A single amino acid substitution in human APOBEC3G antiretroviral enzyme confers resistance to HIV-1 virion infectivity factor-induced depletion. *Proc. Natl. Acad. Sci. USA* **101**, 5652–5657 (2004).
16. Huthoff, H. & Malim, M.H. Identification of amino acid residues in APOBEC3G required for regulation by human immunodeficiency virus type 1 Vif and Virion encapsidation. *J. Virol.* **81**, 3807–3815 (2007).
17. Albin, J.S. *et al.* A single amino acid in human APOBEC3F alters susceptibility to HIV-1 Vif. *J. Biol. Chem.* **285**, 40785–40792 (2010).
18. Chen, K.M. *et al.* Structure of the DNA deaminase domain of the HIV-1 restriction factor APOBEC3G. *Nature* **452**, 116–119 (2008).
19. Furukawa, A. *et al.* Structure, interaction and real-time monitoring of the enzymatic reaction of wild-type APOBEC3G. *EMBO J.* **28**, 440–451 (2009).
20. Holden, L.G. *et al.* Crystal structure of the anti-viral APOBEC3G catalytic domain and functional implications. *Nature* **456**, 121–124 (2008).
21. Shandilya, S.M. *et al.* Crystal structure of the APOBEC3G catalytic domain reveals potential oligomerization interfaces. *Structure* **18**, 28–38 (2010).
22. Betts, L., Xiang, S., Short, S.A., Wolfenden, R. & Carter, C.W.J. Cytidine deaminase. The 2.3 Å crystal structure of an enzyme: transition-state analog complex. *J. Mol. Biol.* **235**, 635–656 (1994).
23. Prochnow, C., Bransteitter, R., Klein, M.G., Goodman, M.F. & Chen, X.S. The APOBEC-2 crystal structure and functional implications for the deaminase AID. *Nature* **445**, 447–451 (2007).
24. Krzysiak, T.C., Jung, J., Thompson, J., Baker, D. & Gronenborn, A.M. APOBEC2 is a monomer in solution: implications for APOBEC3G models. *Biochemistry* **51**, 2008–2017 (2012).
25. Iwatani, Y. *et al.* HIV-1 Vif-mediated ubiquitination/degradation of APOBEC3G involves four critical lysine residues in its C-terminal domain. *Proc. Natl. Acad. Sci. USA* **106**, 19539–19544 (2009).
26. Russell, R.A. & Pathak, V.K. Identification of two distinct human immunodeficiency virus type 1 Vif determinants critical for interactions with human APOBEC3G and APOBEC3F. *J. Virol.* **81**, 8201–8210 (2007).
27. Larue, R.S., Lengyel, J., Jónsson, S.R., Andrésdóttir, V. & Harris, R.S. Lentiviral Vif degrades the APOBEC3Z3/APOBEC3H protein of its mammalian host and is capable of cross-species activity. *J. Virol.* **84**, 8193–8201 (2010).
28. Kitamura, S., Ode, H. & Iwatani, Y. Structural features of antiviral APOBEC3 proteins are linked to their functional activities. *Front. Microbiol.* **2**, 258 (2011).
29. Hultquist, J.F., Binka, M., Larue, R.S., Simon, V. & Harris, R.S. Vif proteins of human and simian immunodeficiency viruses require cellular CBFβ to degrade APOBEC3 restriction factors. *J. Virol.* **86**, 2874–2877 (2012).
30. He, Z., Zhang, W., Chen, G., Xu, R. & Yu, X.F. Characterization of conserved motifs in HIV-1 Vif required for APOBEC3G and APOBEC3F interaction. *J. Mol. Biol.* **381**, 1000–1011 (2008).
31. Pery, E., Rajendran, K.S., Brazier, A.J. & Gabuzda, D. Regulation of APOBEC3 proteins by a novel YXXL motif in human immunodeficiency virus type 1 Vif and simian immunodeficiency virus SIVagm Vif. *J. Virol.* **83**, 2374–2381 (2009).
32. Schröfelbauer, B., Senger, T., Manning, G. & Landau, N.R. Mutational alteration of human immunodeficiency virus type 1 Vif allows for functional interaction with nonhuman primate APOBEC3G. *J. Virol.* **80**, 5984–5991 (2006).
33. Tian, C. *et al.* Differential requirement for conserved tryptophans in human immunodeficiency virus type 1 Vif for the selective suppression of APOBEC3G and APOBEC3F. *J. Virol.* **80**, 3112–3115 (2006).
34. Stauch, B. *et al.* Model structure of APOBEC3C reveals a binding pocket modulating ribonucleic acid interaction required for encapsidation. *Proc. Natl. Acad. Sci. USA* **106**, 12079–12084 (2009).